ACS OMEGA

Open Access

This article is licensed under CC-BY-NC-ND 4.0

http://pubs.acs.org/journal/acsodf

Article

Simulation of High-Viscosity Generalized Newtonian Fluid Flows in the Mixing Section of a Screw Extruder Using the Lattice Boltzmann Model

Liguo Liu, Zhuo Meng,* Yujing Zhang, and Yize Sun

Cite This: *ACS Omega* 2023, 8, 47991−48018

Read Online

ACCESS | Metrics & More | Article Recommendations

ABSTRACT: The mixing quality of polymer melts in the mixing section of a single-screw extruder and an injection molding machine has considerable effects on the properties of the molded products. Therefore, the study of the flow field of polymer melts in the mixing section is of great importance. The lattice Boltzmann method (LBM) exhibits unique advantages in simulating non-Newtonian fluids. Many researchers have used LBM to study the flow of medium- and low-viscosity fluids. In their studies, the Reynolds number of fluid flows is generally moderate. However, polymer melts are typical high-viscosity fluids, and their flow Reynolds number is generally very small. The single-relaxation-time lattice Boltzmann method (SRT−LBM) has been used previously to study the flow field of power law fluids in the mixing section. Herein, the flow field of high-viscosity generalized Newtonian fluids in the mixing section of a single-screw extruder is studied using SRT−LBM, the two-relaxation-time lattice Boltzmann method (TRT−LBM), and the multiple-relaxation-time lattice Boltzmann method (MRT−LBM). Through comparison, TRT−LBM has been found to exhibit obvious advantages regarding stability, calculation accuracy, calculation efficiency, and selection of simulation parameters. The TRT−LBM is more suitable for studying high-viscosity generalized Newtonian fluids than SRT−LBM and MRT−LBM. SRT−LBM has low computational efficiency when simulating high-viscosity generalized Newtonian fluids, and instability is easily caused when the fluid has a yield stress. For MRT−LBM, only by studying the relaxation parameters can its advantages be fully utilized. However, optimizing the accuracy and stability of the MRT−LBM via parameter research and linear stability analysis is difficult. For non-Newtonian fluids, it is difficult to optimize the relaxation parameters to make the MRT−LBM more stable and accurate than the TRT−LBM. It is difficult for the MRT−LBM to realize its potential when simulating high-viscosity generalized Newtonian fluids. In addition, we studied the flow pattern in the cross section of the screw channel and compared it to the results reported in previous studies.

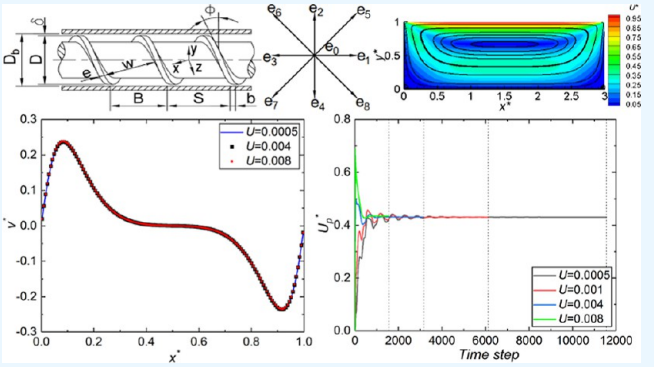

1. INTRODUCTION

Single-screw extruders and injection molding machines have been widely used in the chemical industry. Every year, extruders and injection molding machines process more than 114 million tons of polymer raw materials.[1,2] Extruders are widely used in the production of pipes, plates, profiles, cables, fibers, coatings, and films. Extruders are often used for compounding, mixing, granulation, and chemical reactions of raw materials.[1,2] In addition, extruders are also widely used in food and medicine molding and 3D printing. Injection molding machines are mainly used for the molding of plastic products. Most plastic products are manufactured by injection molding. Most polymers pass through an extrusion line at least once in their life cycle.

The mixing quality of the mixing section of a single-screw extruder and an injection molding machine has considerable effects on the properties of the molded products. However, observing the mixing process of polymer melts in a barrel is difficult. Therefore, using mathematical models to study the mixing process of polymer melts in the mixing section of an extrusion screw is of great importance. Figure 1a shows the mixing section of a standard extrusion screw, and Figure 2a shows the pin mixing section of an extrusion screw. Generally, the height of the screw flight is small compared with the diameter of the barrel. When the effects of the curvature of the screw on the melt flow are ignored, the screw can be considered as a flat rectangular channel.[1,2] According to the

Received: September 4, 2023
Revised: October 30, 2023
Accepted: November 15, 2023
Published: December 7, 2023

ACS Publications

© 2023 The Authors. Published by American Chemical Society

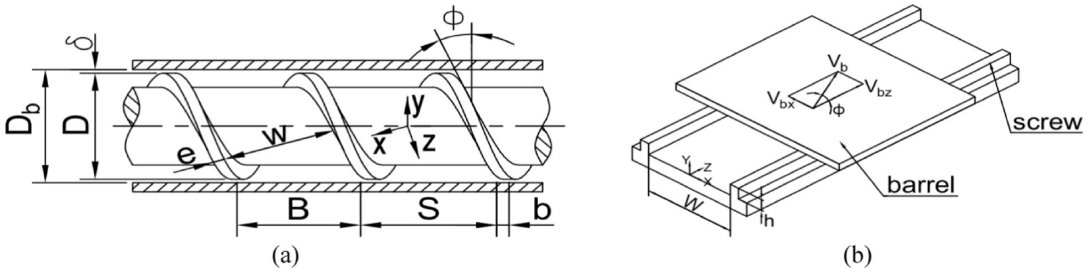

Figure 1. Mixing section of a standard extrusion screw: (a) structure of the mixing section and (b) simplified model.

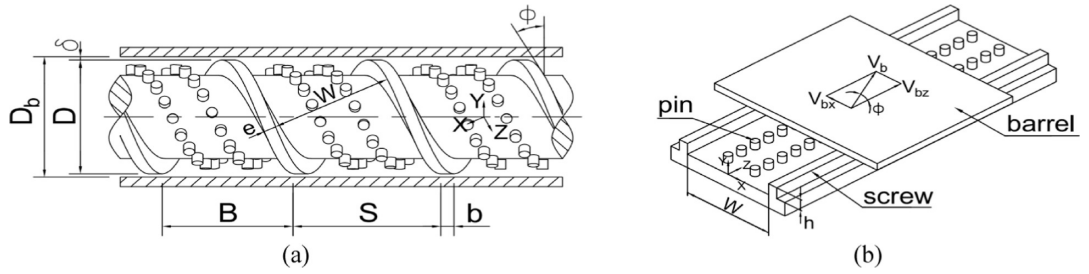

Figure 2. Pin mixing section of an extrusion screw: (a) structure of the pin mixing section and (b) simplified model.

principle of reversed motion, the screw is considered fixed, and the barrel is considered rotated.[2] Therefore, the complex screw mixing section can be simplified into a moving plate and a fixed rectangular channel, as shown in Figures 1b and 2b.

McKelvey[3] considered polymer melts as Newtonian fluids and obtained the analytical solution of the velocity profile along the vertical centerline of the cross section of a screw channel. Yao et al.[4,5] considered polymer melts as Newtonian fluids and numerically simulated the flow field in the cross section of a screw channel with and without pins by using the finite difference method (FDM). Yao et al.[4,5] designed a visualization experiment device and conducted an experimental study using high-viscosity corn syrup. The experimental results verified the simulation results. Horiguchi et al.[6] used the lattice gas method (LGM) to numerically simulate the flow pattern in the cross section of a screw channel with and without pins. The numerical results agree well with the visualization experimental results of Yao et al.[4,5] Horiguchi et al.[6] compared the numerical results of the velocity profile along the vertical centerline of the cross section of the screw channel with McKelvey's analytical solution. By comparison, the numerical results using the LGM were found to be more accurate than those using the FDM. However, some differences were observed between the numerical solution obtained using the LGM and McKelvey's analytical solution. Buick and Cosgrove[7] used the single-relaxation-time lattice Boltzmann method (SRT−LBM) to study the flow field of Newtonian fluids in the cross section of a screw channel. By comparison, the SRT−LBM was found to be more effective and accurate than the LGM. Generally, polymer melts exhibit non-Newtonian properties. Buick and Cosgrove[8,9] used the SRT−LBM to study the flow field of power law fluids in the cross section of the screw channel. They compared the effects of the power law index on the distribution of velocity and shear rates and pointed out that the LBM has unique advantages in simulating non-Newtonian fluids.

The LBM is simple to program, convenient to calculate, and naturally parallel. The LBM with a BGK collision operator is called the SRT−LBM.[10] The SRT−LBM is simple, efficient, and very popular. For Newtonian fluid with medium Reynolds number, the SRT model is the simplest and most effective model. However, when the Reynolds number is too large or too small, the SRT−LBM may be divergent, unstable, or inaccurate. When the Reynolds number $Re = |u|N\Delta x/\nu$ is very large, the viscosity $\nu(\gamma)$ needs to be taken as a very small value. According to the formula $\tau = 3\nu(\gamma) + 0.5$, when the viscosity is close to 0, the relaxation time τ is close to 0.5. However, $\tau > 1/2$ is a necessary condition for stability. When τ is close to 0.5, the SRT−LBM will be unstable. When the Reynolds number $Re = |u|N\Delta x/\nu$ is very small, the viscosity $\nu(\gamma)$ needs to be taken as a very large value. According to the formula $\tau = 3\nu(\gamma) + 0.5$, when the viscosity is large, the relaxation time $\tau \gg 1$. It is not recommended to use the relaxation time $\tau \gg 1$ as the numerical errors of the SRT−LBM grow with $(\tau/\Delta t - 1/2)^2$. When the relaxation time $\tau \gg 1$, the SRT−LBM will be inaccurate. D'Humières proposed the multiple-relaxation-time lattice Boltzmann method (MRT−LBM) in 1992.[11] Lallemand and Luo[12] conducted a theoretical study on the MRT model in 2000 and showed that the MRT model can overcome the shortcomings of the SRT model. The MRT model contains many free parameters that can adjust accuracy and stability and is the most general model. The MRT−LBM can effectively simulate high Reynolds number flows. Many scholars have used the MRT−LBM to study high Reynolds number flows.[13−16] However, there are few studies on high-viscosity and low-Reynolds number flows.

In recent years, more and more scholars have used the LBM to study the flow of non-Newtonian fluids.[7−9,17−24] The LBM has greater advantages than the conventional computational fluid dynamics methods when simulating non-Newtonian fluids. When using LBM for simulation, the shear rate tensor can be calculated locally without calculating the velocity gradient. Therefore, the LBM has natural parallelism and can greatly improve the computational efficiency. Deng et al.[25] and Mohebbi et al.[26] compared the LBM with the finite element method (FEM) and found that the LBM considerably saves the calculation time than the FEM. The SRT−LBM has been successfully used in the study of power law fluids. However,

https://doi.org/10.1021/acsomega.3c06663
ACS Omega 2023, 8, 47991−48018

when the power law index is too large or too small, the SRT−LBM may be inaccurate and unstable. The apparent viscosity of non-Newtonian fluids is related to the shear rate. The relaxation time τ of the SRT−LBM is determined by the apparent viscosity of the fluid domain. If the apparent viscosity is too large, then $\tau \gg 1$, and the SRT−LBM may be inaccurate.[27] When the apparent viscosity is too small, then τ approaches 0.5, and the SRT−LBM may be unstable.[28] Therefore, some scholars have improved the SRT−LBM.[29−32] However, these improved models are mostly for power law fluids, and their effectiveness for other non-Newtonian fluids has not been verified.

Chai et al.[33] used the MRT model for the first time to study generalized Newtonian fluids. Li et al.[34] studied the flow of power law fluids in a two-dimensional square cavity using the MRT model. Bisht and Patil[35] simulated the two-dimensional flow of the power law fluids, Carreau fluids, Carreau−Yasuda fluids, and Cross fluids using the MRT model. Chen et al.[36] studied the two-dimensional Poiseuille flow, lid-driven cavity flow, and sudden expansion flow of Bingham fluids using the MRT model. In addition, they also studied the flow of Bingham fluids around solid particles. Grasinger et al.[37] compared the accuracy and stability of SRT and MRT models in simulating non-Newtonian fluids. In their study, the Reynolds number is between 100 and 10,000. They pointed out that the MRT model is more accurate and stable in simulating non-Newtonian fluids but that the MRT model requires more computational time, sometimes 5 times that of the SRT model. Chen et al.[38] studied the three-dimensional Poiseuille flow of Bingham fluids in the circular and square tubes using the MRT model and found that the relaxation parameters of the MRT model have considerable effects on the accuracy and stability of the simulation, and only by optimizing the relaxation parameters reasonably can the high-precision results be obtained. However, the MRT model, especially three-dimensional model, contains many relaxation parameters, which are difficult to optimize.[39] In previous studies, the same set of relaxation parameters was chosen, and the optimization method of relaxation parameters was not given.[33−37]

Ginzburg[40] proposed the two-relaxation-time lattice Boltzmann method (TRT−LBM) in 2005. The TRT−LBM has two relaxation times, τ^+ and τ^-. τ^+ is related to the apparent viscosity of the fluid. τ^- is a free parameter. The magic parameter, Λ, is a function of τ^+ and τ^-. When the TRT−LBM is used for simulation, if the viscosity changes, just by adjusting the relaxation time τ^- to keep the magic parameter fixed, the accuracy error can be independent of the viscosity. The TRT model is as simple and efficient as the SRT model, while absorbing the advantages of the accuracy and stability of the MRT model.[41−43] At present, the TRT model has not received sufficient attention and is not as popular as the SRT and MRT models.[39] With the continuous deepening of research, the advantages of the TRT model are gradually evident, and the TRT model is being used more and more widely.[44−47]

First, we use the TRT model to study the flow of generalized Newtonian fluids in a lid-driven cavity and verify the validity of the TRT model. Second, the velocity profiles of high-viscosity power law fluids and Bingham fluids in the cross section of a screw channel are studied using the SRT and TRT models, respectively. The stability, calculation accuracy, and calculation efficiency of the SRT and TRT models are compared in detail. Third, the MRT model is used to study the high-viscosity power law fluids in the screw channel. The effectiveness of the MRT model for high-viscosity generalized Newtonian fluids is further studied. Finally, the flow patterns of the generalized Newtonian fluids in the cross section of the screw channel are studied using the TRT model. The results of the TRT model are compared with the simulation results of Buick et al.[7−9] and the visualization experiment results of Yao et al.[4,5] In addition, we use the TRT model to study the flow patterns of generalized Newtonian fluids in the pin mixing section of the screw channel and compare it with the visualization experimental results of Yao et al.[4,5]

2. CONSTITUTIVE EQUATIONS OF GENERALIZED NEWTONIAN FLUIDS

The polymer melt has viscoelastic characteristics. In many cases, the elastic effect of polymer melts can be ignored. Whether the elastic effect of the polymer melt can be ignored needs to be determined according to the specific application. Generally, when the flow field in the extruder is studied, the elastic effect of the polymer melt can be ignored. The generalized Newtonian fluid model can describe the rheological properties of the polymer melt well and is widely used in the flow field analysis of polymer processing.[1]

2.1. Power Law Model. The apparent viscosity of power law fluids is defined by[48]

$$\nu_P(\gamma) = m|\gamma|^{n-1} \tag{1}$$

where m represents the flow consistency coefficient of the fluid, n represents the power law index of the fluid, and γ represents the shear rate tensor. The power law fluids include shear-thinning fluids ($n < 1$) and shear-thickening fluids ($n > 1$). If $n = 1$, then the power law fluids become the Newtonian fluids.

2.2. Bingham Plastic Model. The constitutive equations of the Bingham model have been proposed by Bird,[49] which can be expressed as

$$\begin{cases} \tau = \left(\dfrac{\tau_B}{|\gamma|} + \mu_B\right)\gamma & |\tau| \geq \tau_B \\ \gamma = 0 & |\tau| < \tau_B \end{cases} \tag{2}$$

where τ represents the shear stress tensor, τ_B represents the Bingham yield stress, and μ_B represents the plastic viscosity. When $\tau_B = 0$, the fluid is a Newtonian fluid. Papanastasiou[50] proposed a modified equation to overcome the discontinuity of eq 2, which can be expressed as

$$\tau = \left[\mu_B + (1-e^{-m|\gamma|})\frac{\tau_B}{|\gamma|}\right]\gamma \tag{3}$$

where m represents the stress growth exponent. When m is large enough, eq 3 can be well approximated to eq 2.

The apparent viscosity of the Bingham plastic model can be determined by eq 3

$$\nu_B(\gamma) = \frac{\tau}{\gamma} = \mu_B + (1 - e^{-m|\gamma|})\frac{\tau_B}{|\gamma|} \tag{4}$$

3. NUMERICAL METHOD

3.1. SRT−LBM. The evolution equation of SRT−LBM can be expressed as

https://doi.org/10.1021/acsomega.3c06663
ACS Omega 2023, 8, 47991−48018

$$f_i(x + e_i\Delta t, t + \Delta t) = f_i(x, t) + \Omega_i(x, t), \quad (i = 0 - 8) \tag{5}$$

where Ω_i is the collision operator and e_i are the discrete velocities in the D2Q9 model (see Figure 3), which can be determined as

$$e_i = \begin{cases} (0,0) & i = 0 \\ [\cos[(i-1)\pi/2], \sin[(i-1)\pi/2]] & i = 1,2,3,4 \\ \sqrt{2}\left[\cos\left(\frac{(i-1)\pi}{2} + \pi/4\right), \sin\left(\frac{(i-1)\pi}{2} + \pi/4\right)\right] & i = 5,6,7,8 \end{cases} \tag{6}$$

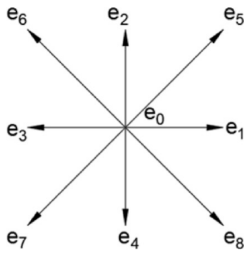

Figure 3. Discrete velocity vectors at a grid site in the D2Q9 model.

The BGK collision operator of the SRT model can be expressed as[51]

$$\Omega_i(x, t) = -\frac{\Delta t}{\tau}[f_i(x, t) - f_i^{eq}(x, t)] \tag{7}$$

where f_i represents the distribution function of e_i and f_i^{eq} represents the equilibrium distribution function for the D2Q9 lattice, which can be expressed as[39]

$$f_i^{eq}(x, t) = \omega_i\rho\left[1 + \frac{e_i \cdot u}{c_s^2} + \frac{(e_i \cdot u)^2}{2c_s^4} - \frac{u^2}{2c_s^2}\right] \tag{8}$$

where $\omega_0 = 4/9$, $\omega_i = 1/9 (i = 1-4)$, $\omega_i = 1/36 (i = 5-8)$, and $c_s = 1/\sqrt{3}$ is the sound speed.

The relaxation time, τ, depends on the kinematic viscosity, which can be determined by

$$\tau = 3\nu(\gamma) + \frac{1}{2} \tag{9}$$

The evolutionary progress of the SRT model includes the following two steps:

(1) the collision step

$$f_i^*(x, t) = f_i(x, t) - \frac{\Delta t}{\tau}[f_i(x, t) - f_i^{eq}(x, t)] \tag{10}$$

where $f_i^*(x,t)$ represents the distribution function after the collision; and

(2) the propagation step

$$f_i(x + e_i\Delta t, t + \Delta t) = f_i^*(x, t) \tag{11}$$

The macroscopic density, ρ, and velocity, u, at each node can be determined directly as

$$\rho(x, t) = \sum_{i=0}^{8} f_i(x, t), \; u(x, t) = \frac{1}{\rho(x, t)} \sum_{i=0}^{8} e_i f_i(x, t) \tag{12}$$

3.2. TRT−LBM. The evolution equation of the TRT−LBM can be expressed as

$$f_i(x + e_i\Delta t, t + \Delta t) = f_i(x, t) + \Omega_i(x, t) \quad (i = 0 - 8) \tag{13}$$

where Ω_i is the collision operator and e_i are the discrete velocities in the D2Q9 model (see Figure 3), which can be determined by eq 6.

The distribution function of the TRT model includes the symmetric and antisymmetric parts

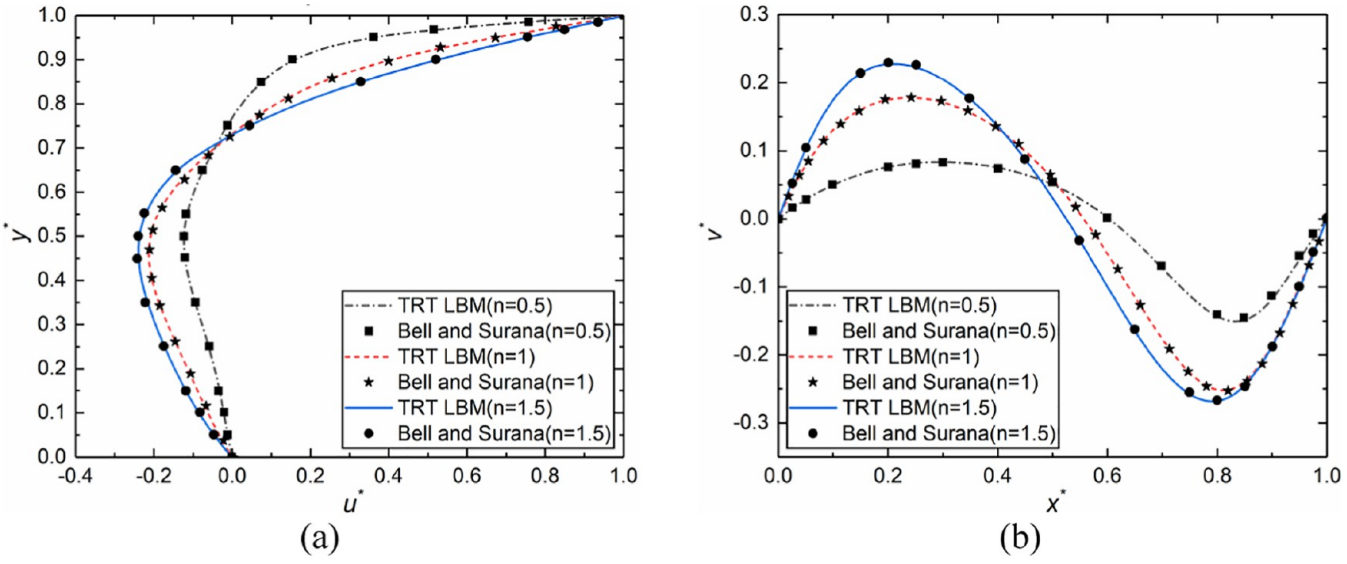

Figure 4. Comparison of TRT−LBM results of power law fluids with those of previous studies.[55] (a) Distributions of u-velocity along the vertical centerline of the simulation domain. (b) Distributions of v-velocity along the horizontal centerline of the simulation domain.

https://doi.org/10.1021/acsomega.3c06663
ACS Omega 2023, 8, 47991−48018

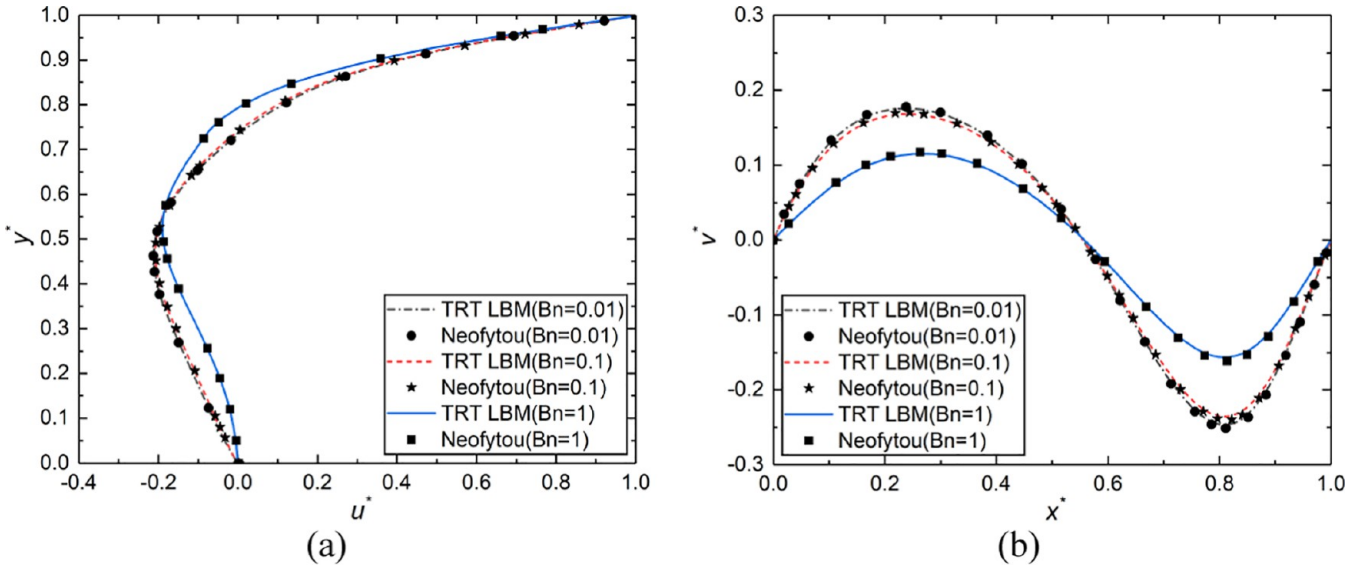

Figure 5. Comparison of TRT−LBM results of Bingham fluids with those of previous studies.[56] (a) Distributions of u-velocity along the vertical centerline of the simulation domain. (b) Distributions of v-velocity along the horizontal centerline of the simulation domain.

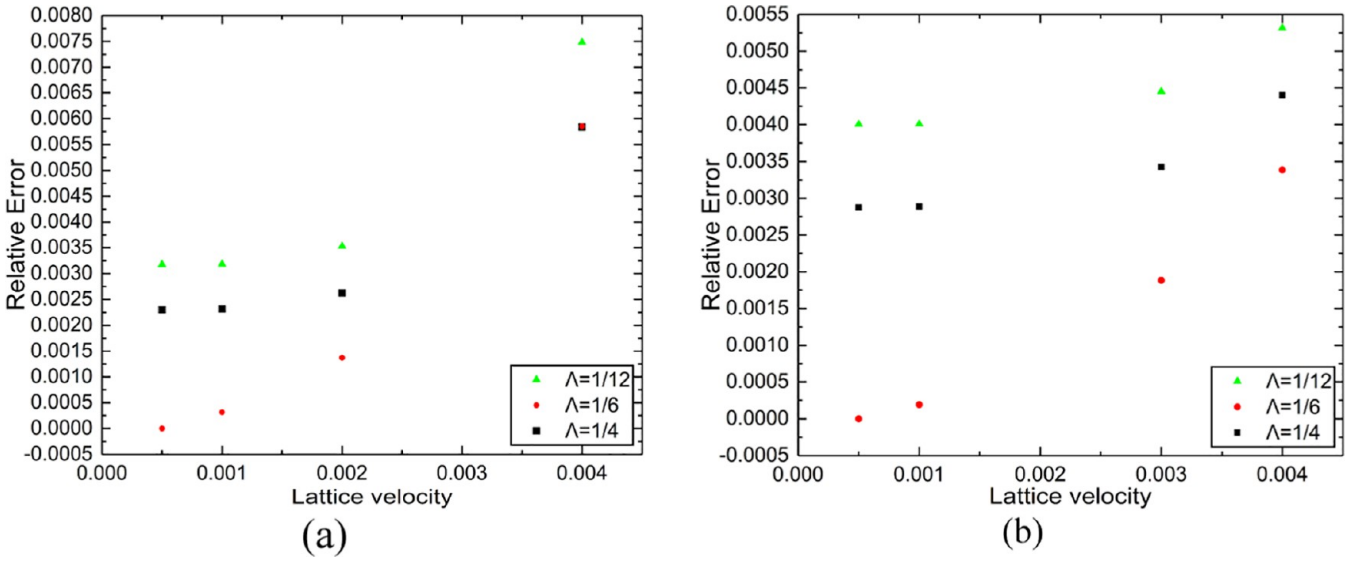

Figure 6. Comparison of simulation accuracy of the TRT−LBM under different magic parameters, Λ. (a) Power law fluids (n = 1.5) and (b) Bingham fluids (Bn = 1.5).

$$f_i = f_i^+ + f_i^-, \qquad f_{\bar{i}} = f_i^+ - f_i^- \tag{14}$$

where f_i represents the distribution function of $\boldsymbol{e}_i$, $f_{\bar{i}}$ represents the distribution function of $\boldsymbol{e}_{\bar{i}} = -\boldsymbol{e}_i$, and f_i^+ and f_i^- represent the symmetric and antisymmetric parts of the distribution function, respectively, which can be determined by

$$f_i^+ = \frac{1}{2}(f_i + f_{\bar{i}}), \qquad f_i^- = \frac{1}{2}(f_i - f_{\bar{i}}) \tag{15}$$

The equilibrium distribution function f_i^{eq} of the D2Q9 TRT model can be expressed by eq 8.

The equilibrium distribution function of the TRT model includes the symmetric and antisymmetric parts

$$f_i^{eq} = f_i^{eq+} + f_i^{eq-}, \qquad f_{\bar{i}}^{eq} = f_i^{eq+} - f_i^{eq-} \tag{16}$$

where f_i^{eq} represents the equilibrium distribution function of $\boldsymbol{e}_i$, $f_{\bar{i}}^{eq}$ represents the equilibrium distribution function of $\boldsymbol{e}_{\bar{i}} = -\boldsymbol{e}_i$, and f_i^{eq+} and f_i^{eq-} represent the symmetric and antisymmetric parts of the equilibrium distribution function, respectively, which can be expressed as

$$f_i^{eq+} = \frac{1}{2}(f_i^{eq} + f_{\bar{i}}^{eq}), \qquad f_i^{eq-} = \frac{1}{2}(f_i^{eq} - f_{\bar{i}}^{eq}) \tag{17}$$

The relaxation time, τ^+, depends on the kinematic viscosity, which can be determined by

$$\tau^+ = 3\nu(\gamma) + \frac{1}{2} \tag{18}$$

The magic parameter, Λ, connects the relaxation rate ω^+ to ω^-

$$\Lambda = \left(\frac{1}{\omega^+} - \frac{1}{2}\right)\left(\frac{1}{\omega^-} - \frac{1}{2}\right) \tag{19}$$

where $\omega^+ = 1/\tau^+$ and $\omega^- = 1/\tau^-$.

https://doi.org/10.1021/acsomega.3c06663
ACS Omega 2023, 8, 47991−48018

The relaxation time, τ^-, can be derived from eqs 18 and 19, which can be expressed as

$$\tau^- = \frac{2\Lambda}{2\tau^+ - 1} + \frac{1}{2} \tag{20}$$

The collision operator Ω_i of the TRT model can be expressed as[40]

$$\Omega_i(x, t) = -\omega^+[f_i^+(x, t) - f_i^{eq+}(x, t)] - \omega^-[f_i^-(x, t) - f_i^{eq-}(x, t)] \tag{21}$$

The evolutionary progress of the TRT model includes the following two steps:

(1) the collision step

$$f_i^*(x, t) = f_i(x, t) - \omega^+[f_i^+(x, t) - f_i^{eq+}(x, t)] - \omega^-[f_i^-(x, t) - f_i^{eq-}(x, t)] \tag{22}$$

where $f_i^*(x,t)$ represents the distribution function after the collision; and

(2) the propagation step

$$f_i(x + e_i\Delta t, t + \Delta t) = f_i^*(x, t) \tag{23}$$

The macroscopic velocity, $\boldsymbol{u}$, and density, ρ, at each node can be calculated directly from eq 12.

3.3. MRT−LBM. The evolution equation of the MRT−LBM can be expressed as[12]

$$f_i(x + e_i\Delta t, t + \Delta t) - f_i(x, t) = -M^{-1}SM[f_i - f_i^{eq}] \tag{24}$$

where f_i and f_i^{eq} are the distribution function and equilibrium distribution function of e_i, respectively, M is the transformation matrix, and S is the diagonal relaxation matrix.

The f_i^{eq} of the D2Q9MRT model can be expressed as in eq 8.

The M in the D2Q9MRT model is given by[12]

$$M = \begin{bmatrix} 1 & 1 & 1 & 1 & 1 & 1 & 1 & 1 & 1 \\ -4 & -1 & -1 & -1 & -1 & 2 & 2 & 2 & 2 \\ 4 & -2 & -2 & -2 & -2 & 1 & 1 & 1 & 1 \\ 0 & 1 & 0 & -1 & 0 & 1 & -1 & -1 & 1 \\ 0 & -2 & 0 & 2 & 0 & 1 & -1 & -1 & 1 \\ 0 & 0 & 1 & 0 & -1 & 1 & 1 & -1 & -1 \\ 0 & 0 & -2 & 0 & 2 & 1 & 1 & -1 & -1 \\ 0 & 1 & -1 & 1 & -1 & 0 & 0 & 0 & 0 \\ 0 & 0 & 0 & 0 & 0 & 1 & -1 & 1 & -1 \end{bmatrix} \tag{25}$$

The S of the D2Q9MRT model can be defined as

$$S = \mathrm{diag}(0, s_e, s_\varepsilon, 0, s_q, 0, s_q, s_v, s_v) \tag{26}$$

The relation between the kinematic viscosity and relaxation time, τ, can be expressed as

$$v(\gamma) = c_s^2\left(\frac{1}{s_v} - \frac{1}{2}\right)\delta_t, \qquad s_v = \frac{1}{\tau} \tag{27}$$

where $c_s = 1/\sqrt{3}$.

M is used to change f_i and f_i^{eq} of e_i to the moment space with $m = Mf$ and $m^{eq} = Mf^{eq}$.

$$m = [\rho, e, \varepsilon, j_x, q_x, j_y, q_y, p_{xx}, p_{xy}]^T \tag{28}$$

$$m^{eq} = \rho[1, -2 + 3u^2, 1 - 3u^2, u, -u, v, -v, u^2 - v^2, uv], \quad \boldsymbol{u} = (u, v) \tag{29}$$

The evolutionary progress of the MRT model includes the following two steps:

(1) the collision step

Unlike the SRT and TRT models, the collision step of the MRT model is performed in the moment space

$$f_i^*(x, t) = f_i(x, t) - M^{-1}SM[f_i - f_i^{eq}] \tag{30}$$

where $f_i^*(x,t)$ represents the distribution function after the collision.

(2) the propagation step

$$f_i(x + e_i\Delta t, t + \Delta t) = f_i^*(x, t) \tag{31}$$

The macroscopic velocity, $\boldsymbol{u}$, and density, ρ, at each node can be calculated directly from eq 12.

3.4. Generalized Newtonian Fluid Simulation. The apparent viscosities of power law fluids and Bingham fluids are determined by eqs 1 and 4, respectively. The shear rate γ at each node can be defined as

$$\gamma = \sqrt{2D_{II}} \tag{32}$$

where D_{II} represents the second invariant of the strain-rate tensor, which can be defined as

$$D_{II} = \sum_{\alpha,\beta=1}^{2} S_{\alpha\beta}S_{\alpha\beta} \tag{33}$$

with $S_{\alpha\beta}$ representing the strain-rate tensor at each node.

The $S_{\alpha\beta}$ for the SRT and TRT models can be expressed as[52]

$$S_{\alpha\beta} = -\frac{1}{2\rho c_s^2\tau^+\Delta t}\sum_{i=0}^{8} \boldsymbol{e}_{i\alpha}\boldsymbol{e}_{i\beta}[f_i(\boldsymbol{x}, t) - f_i^{eq}(\boldsymbol{x}, t)] \tag{34}$$

The $S_{\alpha\beta}$ for the MRT model can be expressed as[33]

$$S_{\alpha\beta} = -\frac{1}{2\rho c_s^2\Delta t}\sum_{i=0}^{8} \boldsymbol{e}_{i\alpha}\boldsymbol{e}_{i\beta}\sum_{j=0}^{8} (M^{-1}SM)_{ij}[f_i(x, t) - f_i^{eq}(x, t)] \tag{35}$$

3.5. Boundary Conditions. As shown in Figures 1b and 2b, to compare with the results of previous studies, we ignore the longitudinal velocity component of the screw channel and study only the flow field in the cross section of the screw channel. The upper boundary is a moving boundary with a constant velocity, and all other boundaries of the screw channel are stationary. The boundaries of the pins are stationary. The halfway bounce-back[53,54] boundary conditions were applied at moving and stationary walls. The distribution function on the boundary can be calculated by

$$f_{\bar{i}}(x_b, t + \Delta t) = f_i^*(x_b, t) - 2w_i\rho_w\frac{\boldsymbol{e}_i\cdot\boldsymbol{u}_w}{c_s^2} \tag{36}$$

where $f_{\bar{i}}$ is the distribution function of $e_{\bar{i}} = -e_i$, $f_i^*$is the distribution function after collision, and ρ_w and $\boldsymbol{u}_w$ are the density and velocity, respectively, at the wall location

https://doi.org/10.1021/acsomega.3c06663
ACS Omega 2023, 8, 47991−48018

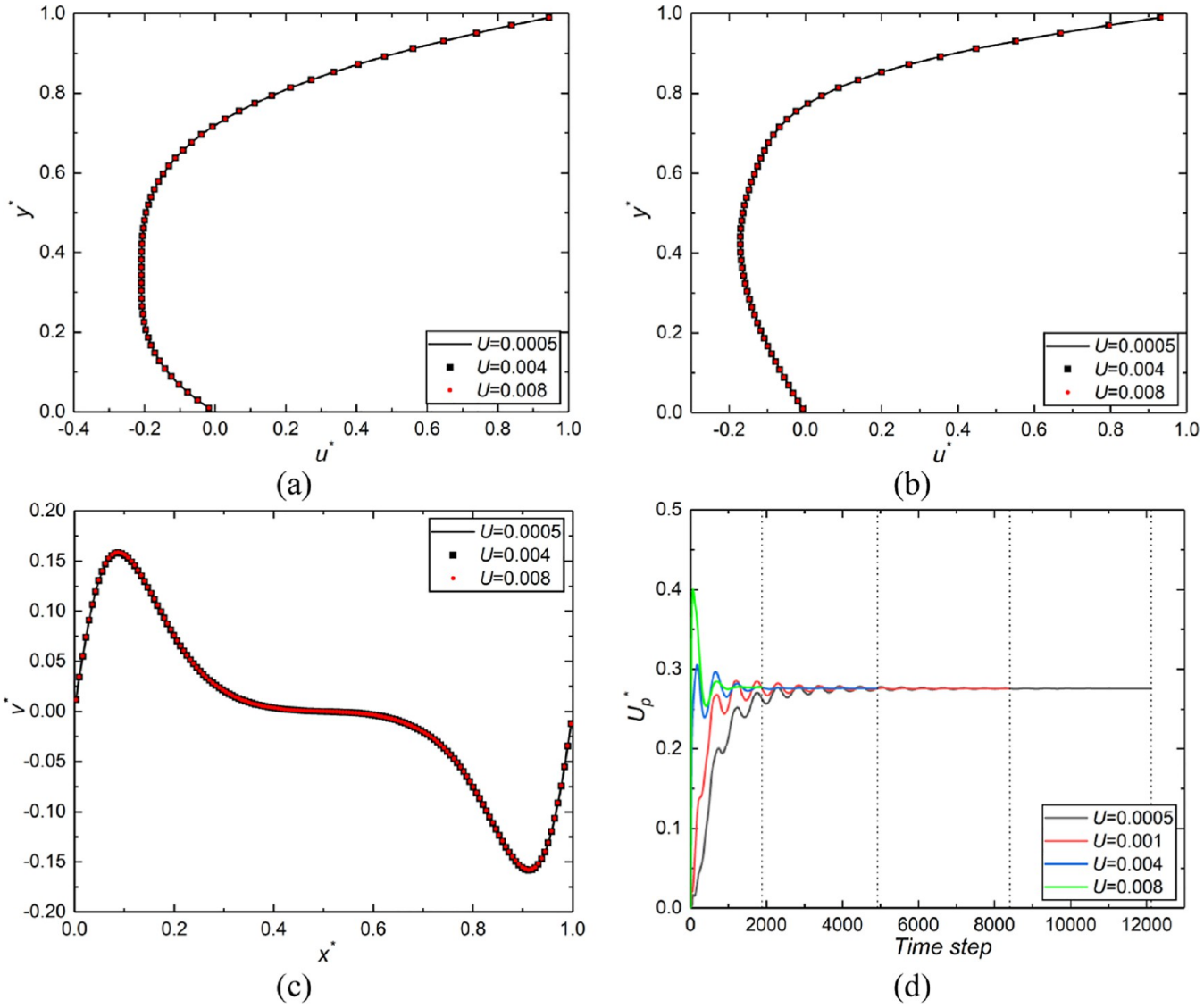

Figure 7. Simulation results of the TRT−LBM for power law fluids at n = 0.5 (Re_p = 0.144). (a) Distributions of u-velocity along the vertical centerline of the simulation domain. (b) Distributions of u-velocity along vertical line x = 25 of the simulation domain. (c) Distributions of v-velocity along the horizontal centerline of the simulation domain. (d) Velocity U_p* that varies with time step at the grid point (25, 45).

$x_w = x_b + \frac{1}{2}e_i\Delta t$. For stationary walls, eq 36 can be simplified as

$$f_{\bar{i}}(x_b, t + \Delta t) = f_i^*(x_b, t) \tag{37}$$

3.6. Dimensionless Parameters. According to similarity theory, the physical conditions of the fluid flow in the screw channel can be defined by dimensionless parameters. The dimensionless spatial coordinates and fluid velocities can be defined as

$$x^* = \frac{x}{H}, \quad y^* = \frac{y}{H}, \quad u^* = \frac{u}{V_{bx}}, \quad v^* = \frac{v}{V_{bx}}, \quad U^* = \sqrt{(u^*)^2 + (v^*)^2} \tag{38}$$

where W represents the width of the screw channel, H represents the height of the screw flight, and V_{bx} represents the lateral velocity component of the screw channel.

The dimensionless shear rate can be defined as

$$\dot{\gamma}^* = \frac{H}{V_{bx}}|\gamma| \tag{39}$$

The Reynolds number of the power law fluids can be defined as

$$Re_p = \frac{{V_{bx}}^{2-n}H^n}{m} \tag{40}$$

where m and n represent the flow consistency coefficient of the fluid and the power law index of the fluid, respectively.

The Reynolds number and Bingham number of the Bingham fluids can be defined as

$$Re_B = \frac{V_{bx}H}{\mu_B}, \quad Bn = \frac{\tau_B H}{\mu_B V_{bx}} \tag{41}$$

where τ_B and μ_B represent the Bingham yield stress and plastic viscosity, respectively.

3.7. Numerical Procedure of the LBM of Generalized Newtonian Fluids. The program execution process of the TRT model of generalized Newtonian fluids is as follows. The

https://doi.org/10.1021/acsomega.3c06663
ACS Omega 2023, 8, 47991−48018

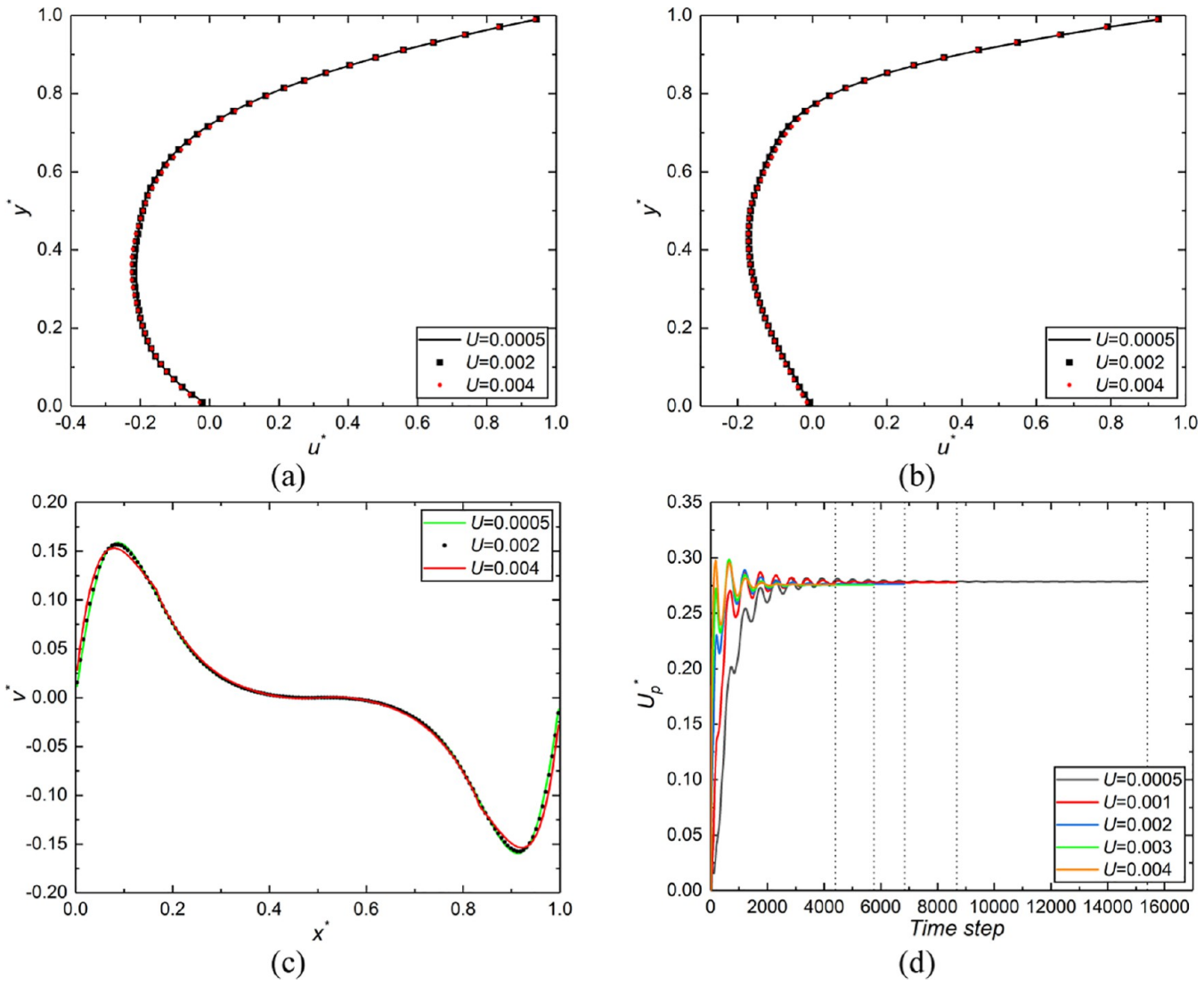

Figure 8. Simulation results of the SRT−LBM for power law fluids at n = 0.5 (Re_p = 0.144). (a) Distributions of u-velocity along the vertical centerline of the simulation domain. (b) Distributions of u-velocity along vertical line x = 25 of the simulation domain. (c) Distributions of v-velocity along the horizontal centerline of the simulation domain. (d) Velocity U_p* that varies with time step at the grid point (25, 45).

program execution process of the SRT and MRT models is similar to that of the TRT model. Herein, MATLAB 2018a software is used for calculation.

(1) Initialize the density and velocity of the fluid domain, by setting $\rho(x,t) = 1$ and $\boldsymbol{u}(x,t) = 0$. $f_i^{eq}(\boldsymbol{x},t)$ can be calculated by eq 8. Initialize the distribution function, by setting $f_i(x,t) = f_i^{eq}(\boldsymbol{x},t)$.

(2) f_i^+ and f_i^- can be determined by eq 15, and f_i^{eq+} and f_i^{eq-}can be determined by eq 17.

(3) The collision step can be implemented by eq 22.

(4) The propagation step can be implemented by eq 23.

(5) The unknown distribution functions at moving and stationary walls can be determined by eqs 36 and 37, respectively.

(6) $S_{\alpha\beta}$ can be calculated by eq 34, D_{II} can be calculated by eq 33, and γ can be determined by eq 32.

(7) The apparent viscosity $\nu(\gamma)$ of power law fluids and Bingham plastic fluids can be calculated by eqs 1 and 4, respectively. τ^+ can be determined by eq 18, and τ^- can be derived from eq 20.

(8) The macroscopic density, ρ, and velocity, $\boldsymbol{u}$, can be determined by eq 12.

(9) Go to step (2) and continue to the next time step. The simulation process ends when the following convergence condition is met:

$$\frac{\sum |U^*(x,\ t+40) - U^*(x,\ t)|}{\sum U^*(x,\ t)} \leq 10^{-6} \tag{42}$$

4. NUMERICAL RESULTS AND DISCUSSION

4.1. Validation of the TRT−LBM for Generalized Newtonian Fluids. At present, the TRT−LBM is not as popular as the SRT−LBM and MRT−LBM. There are few studies on the use of the TRT−LBM to simulate generalized Newtonian fluids flow. To verify the effectiveness of the TRT−LBM in simulating generalized Newtonian fluids, we simulated the fluid flow in a lid-driven cavity.

First, we used the TRT−LBM to study the velocity profiles of power law fluids in a lid-driven cavity at different n values (0.5, 1, and 1.5). The Reynolds number Re_p = 100. As shown

https://doi.org/10.1021/acsomega.3c06663
ACS Omega 2023, 8, 47991−48018

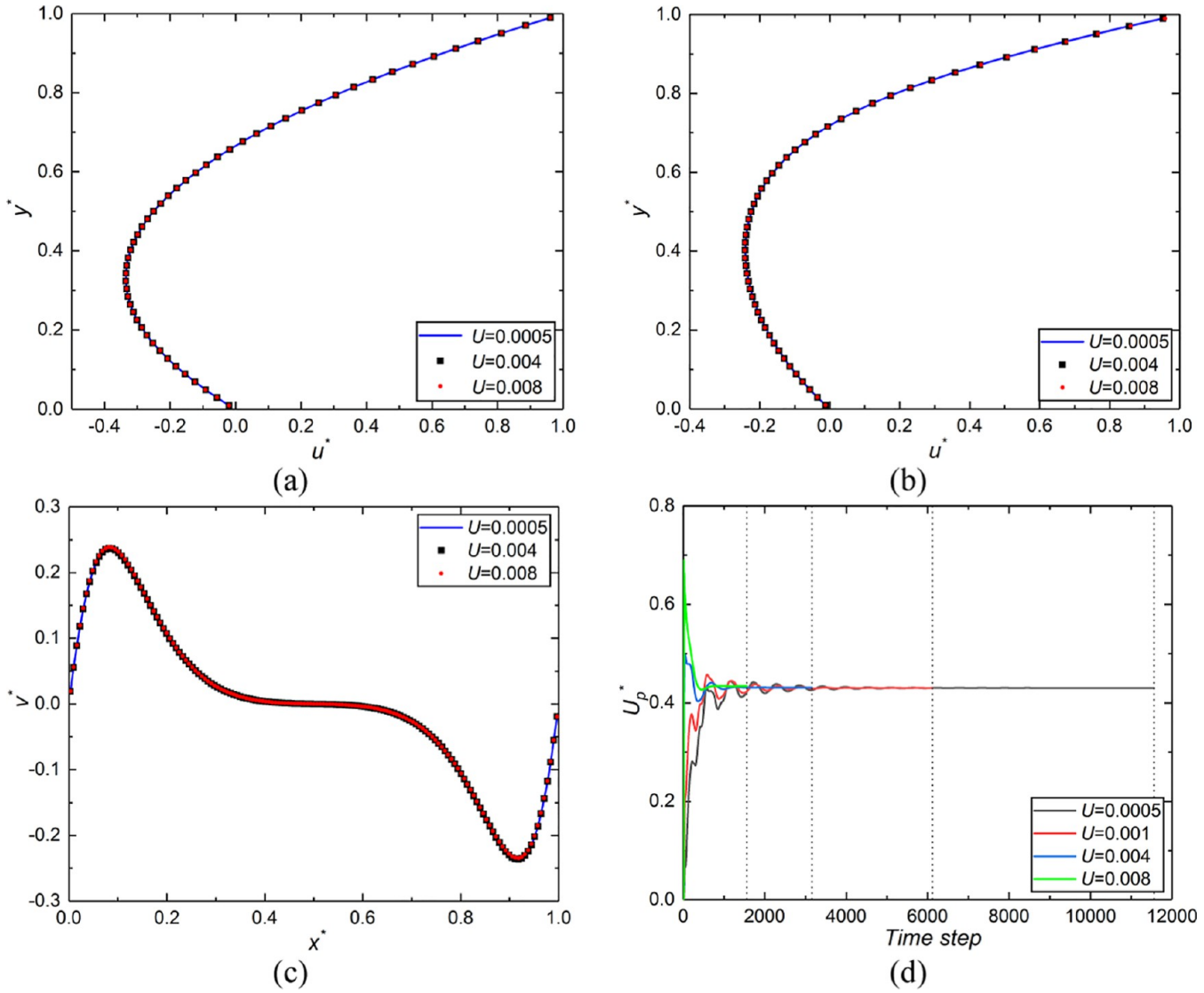

Figure 9. Simulation results of the TRT−LBM for power law fluids at $n = 1$ ($Re_p = 0.144$). (a) Distributions of u-velocity along the vertical centerline of the simulation domain. (b) Distributions of u-velocity along vertical line $x = 25$ of the simulation domain. (c) Distributions of v-velocity along the horizontal centerline of the simulation domain. (d) Velocity U_p* that varies with time step at the grid point (25, 45).

in Figure 4, the results of the TRT−LBM agree well with the results of Bell and Surana.[55]

Subsequently, we used the TRT−LBM to study the velocity profiles of Bingham fluids in a lid-driven cavity at different Bn values (0.01, 0.1, and 1). The Reynolds number $Re_B = 100$. As shown in Figure 5, the results of the TRT−LBM agree well with the results of Neofytou.[56]

4.2. Effectiveness of the TRT− and SRT−LBM for High-Viscosity Generalized Newtonian Fluids. The TRT and SRT models are used to simulate the power law fluids and Bingham fluids in the cross section of the screw channel. The ability of the TRT and SRT models to simulate high-viscosity generalized Newtonian fluids is compared. The simulation accuracy, stability, convergence rate, and selection of simulation parameters of TRT−LBM and SRT−LBM are compared in detail.

Herein, to facilitate the comparison of our results with the results of Horiguchi et al.[6] and Buick et al.,[7−9] the ratio of the width W to height H (W/H) of the screw channel is fixed at 3, and the Reynolds number (Re_p, Re_B) is fixed at 0.144. The upper boundary is a moving boundary, with a constant velocity, and all other boundaries of the screw channel are stationary. The simulation domain is divided into 153 × 51 grid points in the x and y directions. However, the simulation domain is divided into 49 × 16 grid points in the study of Buick et al.[7−9] By numerical simulation, we found that the distribution of u-velocity along the vertical centerline of the simulation domain has high accuracy when the simulation domain is divided into 49 × 16. However, the distribution of v-velocity along the horizontal centerline of the simulation domain has large errors. After verification, the grid point number 153 × 51 is found to be appropriate for deriving grid-independent results.

4.2.1. Selection of Magic Parameter. The magic parameter, Λ, affects the accuracy, stability, and computational efficiency of the simulation. For a given problem, we should try using different magic parameter values to simulate and compare the stability, convergence rate, and accuracy of the simulation process. The more suitable value of the magic parameter is determined by comparison. According to previous research, Λ

https://doi.org/10.1021/acsomega.3c06663
ACS Omega 2023, 8, 47991−48018

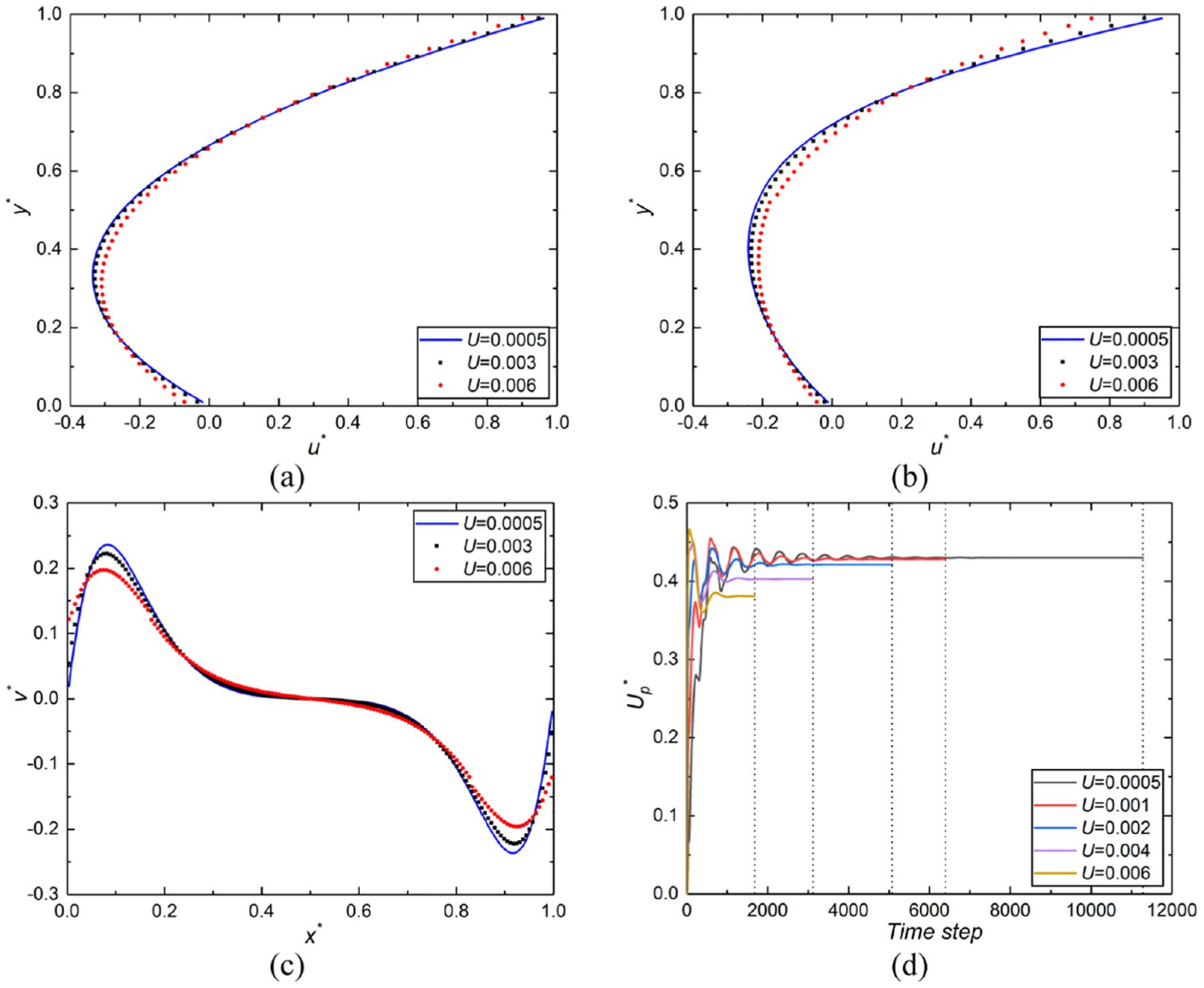

Figure 10. Simulation results of the SRT−LBM for power law fluids at $n = 1$ ($Re_p = 0.144$). (a) Distributions of u-velocity along the vertical centerline of the simulation domain. (b) Distributions of u-velocity along vertical line $x = 25$ of the simulation domain. (c) Distributions of v-velocity along the horizontal centerline of the simulation domain. (d) Velocity U_p^* that varies with time step at the grid point (25, 45).

= 1/12 can cancel the third-order spatial error, Λ = 1/6 can cancel the fourth-order spatial error, and Λ = 1/4 can provide the most stable simulations.

In this paper, the power law fluids (n = 1.5) and Bingham fluids (Bn = 1.5) in the cross section of the screw channel have been studied with different magic parameters Λ (Λ = 1/12, 1/6, and 1/4). To compare the accuracy of the TRT−LBM under different magic parameters Λ, we calculate the relative error. The L_2 error norm can be defined as

$$\mathrm{Err}(U^*) = \sqrt{\frac{\sum_{(x,y)} [U_n^*(x, y) - U_r^*(x, y)]^2}{\sum_{(x,y)} U_r^*(x, y)^2}} \quad (43)$$

where $\mathrm{Err}(U^*)$ represents the relative error, $U_n^*(x,y)$ represents the numerical result of velocity U^*, $U_r^*(x,y)$ represents the reference solution of velocity U^*, and $\sum_{(x,y)}$ represents the sum of all grid points in the simulation domain.

Since there is no analytical solution, we take the numerical results corresponding to the lattice velocity, U = 0.0005, and the magic parameter, Λ = 1/6, as the reference solution, because within a certain range, the smaller the lattice velocity, the higher the simulation accuracy. Figure 6 shows the effects of different magic parameters on the simulation accuracy of TRT−LBM.

Figure 6a shows the effects of different magic parameters and lattice velocity on the simulation accuracy of power law fluids (n = 1.5). As can be seen from Figure 6a, high-accuracy results can be obtained when the magic parameters, Λ, are taken as 1/12, 1/6, and 1/4. For Λ = 1/12, when the lattice velocity, U, is 0.0005, 0.001, 0.002, and 0.004, the corresponding iteration steps are 5880, 4880, 2880, and 1480, respectively. For Λ = 1/6, when the lattice velocity, U, is 0.0005, 0.001, 0.002, and 0.004, the corresponding iteration steps are 5880, 4880, 2880, and 1840, respectively. For Λ = 1/4, when the lattice velocity, U, is 0.0005, 0.001, 0.002, and 0.004, the corresponding iteration steps are 5880, 4880, 2880, and 1800, respectively. It can be found that for the same lattice velocity, U, the convergence rate is almost the same when the magic parameter, Λ, is set to 1/12, 1/6, and 1/4.

Figure 6b shows the effects of different magic parameters and lattice velocity on the simulation accuracy of the Bingham

https://doi.org/10.1021/acsomega.3c06663
ACS Omega 2023, 8, 47991−48018

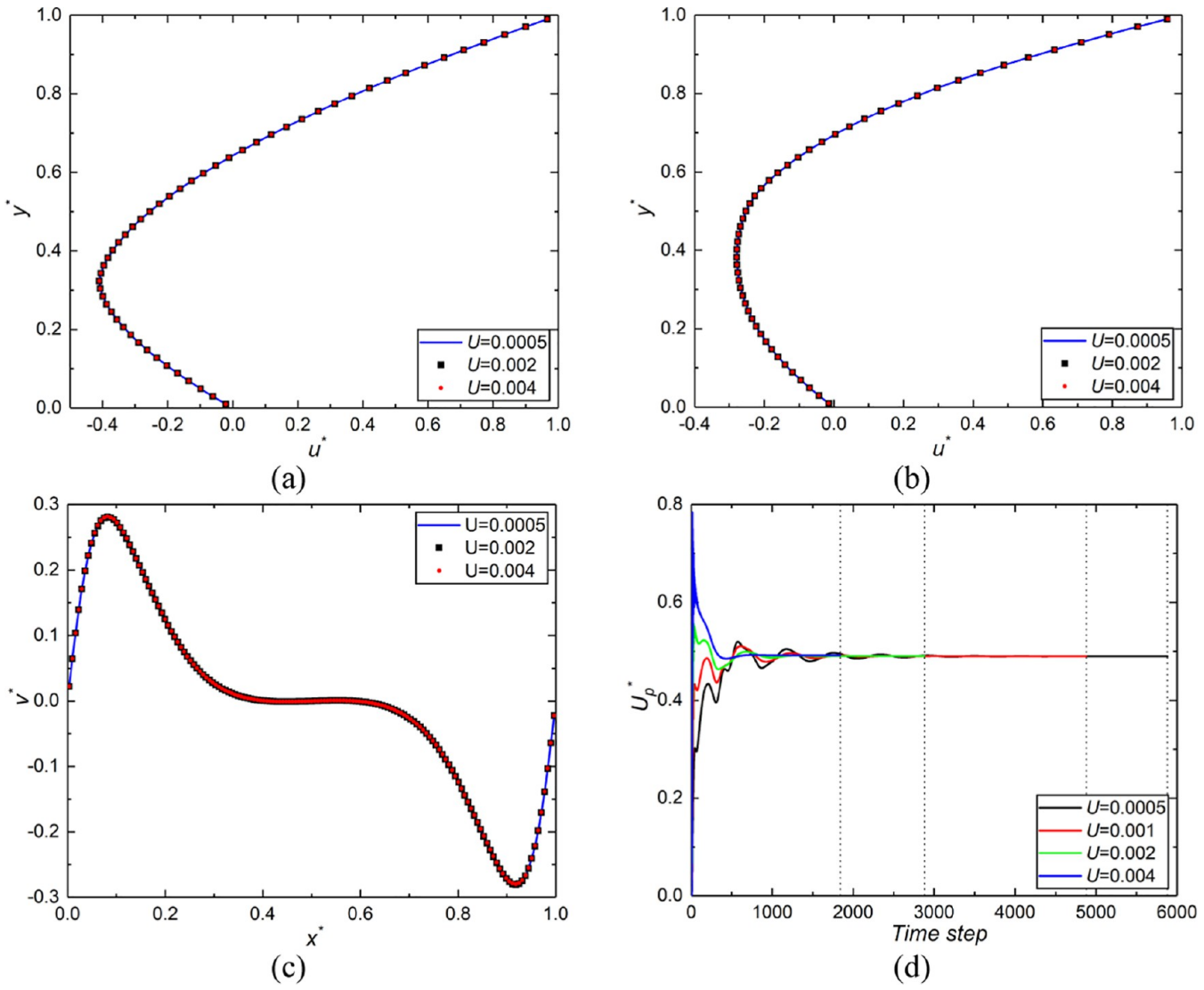

Figure 11. Simulation results of the TRT−LBM for power law fluids at n = 1.5 (Re_p = 0.144). (a) Distributions of u-velocity along the vertical centerline of the simulation domain. (b) Distributions of u-velocity along vertical line x = 25 of the simulation domain. (c) Distributions of v-velocity along the horizontal centerline of the simulation domain. (d) Velocity U_p* that varies with time step at the grid point (25, 45).

fluid (Bn = 1.5). As shown in Figure 6b, high-accuracy results can be obtained when the magic parameters, Λ, are taken as 1/12, 1/6, and 1/4, respectively. For Λ = 1/12, when the lattice velocity, U, is 0.0005, 0.001, 0.003, and 0.004, the corresponding iteration steps are 7760, 5640, 2720, and 1640, respectively. For Λ = 1/6, when the lattice velocity, U, is 0.0005, 0.001, 0.003, and 0.004, the corresponding iteration steps are 7760, 5640, 2720, and 1880, respectively. For Λ = 1/4, when the lattice velocity, U, is 0.0005, 0.001, 0.003, and 0.004, the corresponding iteration steps are 7760, 5640, 2400, and 1880, respectively. It can be found that for the same lattice velocity, U, the convergence rate is almost the same when the magic parameter, Λ, is set to 1/12, 1/6, and 1/4.

Therefore, when the TRT−LBM is used to study the power law fluids and Bingham fluids in the cross section of the screw channel, the magic parameters, Λ, equal to 1/12, 1/6, and 1/4 can all meet the high-accuracy requirements. The computational efficiency is almost the same when the magic parameter, Λ, is set to 1/12, 1/6, and 1/4. In this study, the magic parameter, Λ, is set to 1/6.

4.2.2. Flow of Power Law Fluids in the Cross Section of the Screw Channel. The results of the TRT and SRT models when the power law index n = 0.5, 1, and 1.5 are shown in Figures 7 and 8, 9 and 10, and 11 and 12, respectively. The distributions of u-velocity along the vertical centerline of the simulation domain are shown in Figures 7a−12a, and those along vertical line x = 25 of the simulation domain are shown in Figures 7b−12b. Similarly, the distributions of v-velocity along the horizontal centerline of the simulation domain are shown in Figures 7c−12c, and velocity U_p* that varies with time step at the grid point (25, 45) is shown in Figures 7d−12d. The flow field is steady state. The variation of velocity U_p* with time step is the numerical value generated by the LBM model algorithm during the iteration process.

To compare the accuracy of TRT−LBM and SRT−LBM in simulating power law fluids, we used eq 43 to calculate the relative errors at different lattice velocities. Since there is no analytical solution, we take the numerical results of the TRT−LBM corresponding to the lattice velocity, U = 0.0005, as the reference solution, U_r*(x,y). Because, in general, the smaller the lattice velocity, the higher the simulation accuracy. Figure

https://doi.org/10.1021/acsomega.3c06663
ACS Omega 2023, 8, 47991−48018

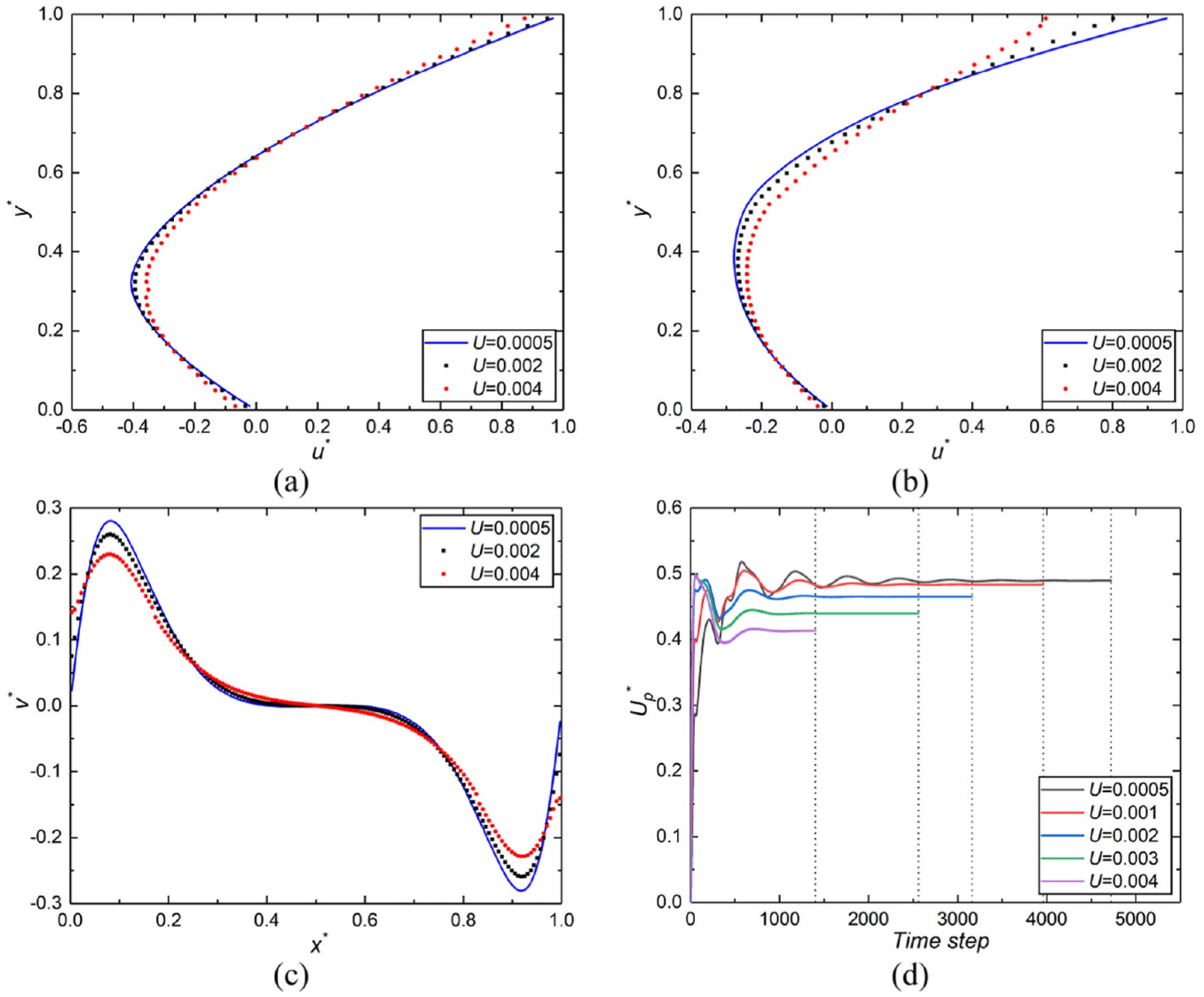

Figure 12. Simulation results of the SRT−LBM for power law fluids at n = 1.5 (Re_p = 0.144). (a) Distributions of u-velocity along the vertical centerline of the simulation domain. (b) Distributions of u-velocity along vertical line x = 25 of the simulation domain. (c) Distributions of v-velocity along the horizontal centerline of the simulation domain. (d) Velocity U_p* that varies with time step at the grid point (25,45).

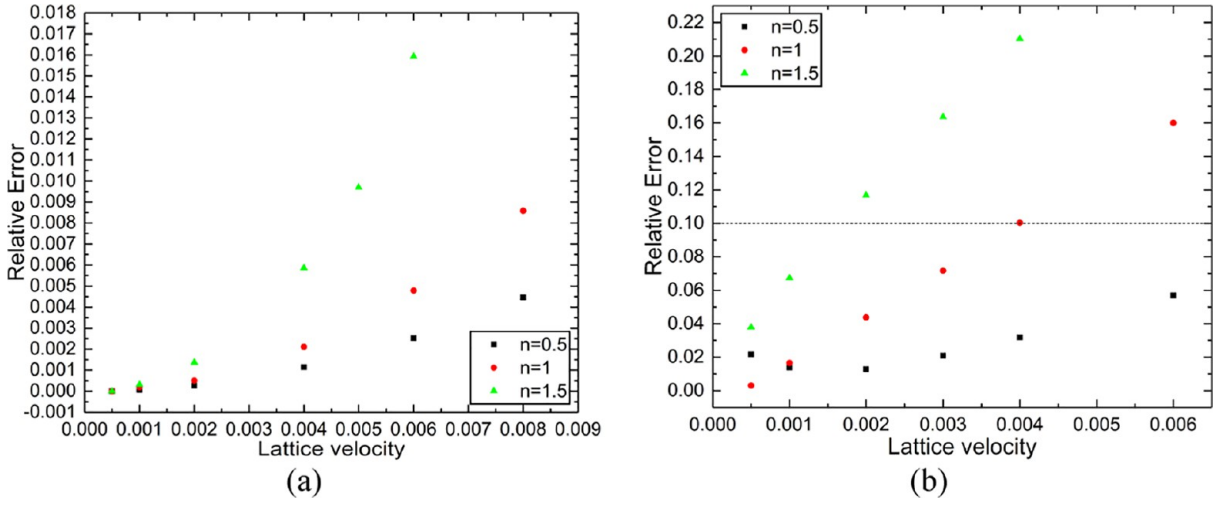

Figure 13. Effects of lattice velocity U on the simulation accuracy of power law fluids. (a) Simulation accuracy of TRT−LBM and (b) Simulation accuracy of SRT−LBM.

https://doi.org/10.1021/acsomega.3c06663
ACS Omega 2023, 8, 47991−48018

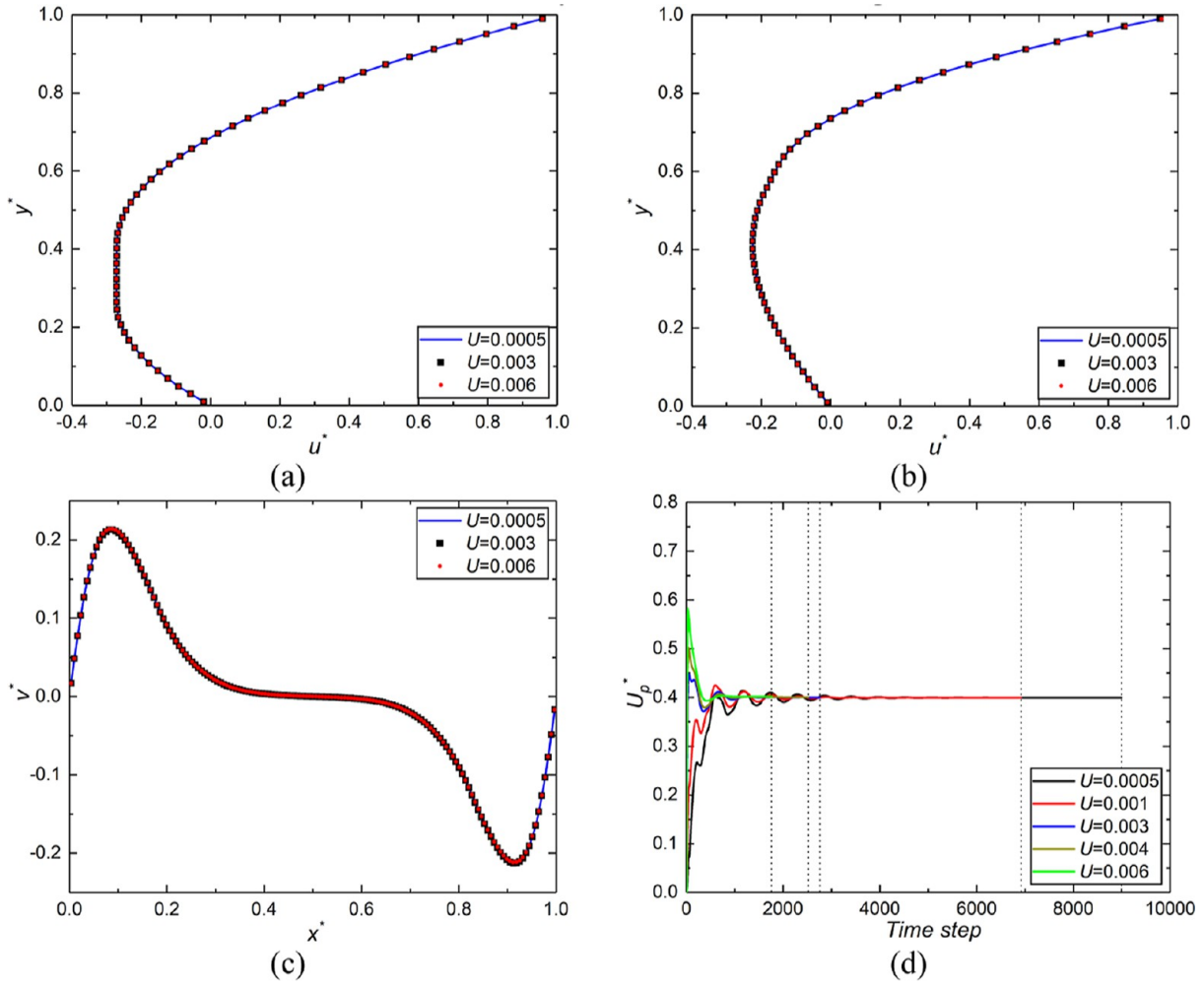

Figure 14. Simulation results of the TRT−LBM for Bingham fluids at Bn = 0.5 (Re_B = 0.144). (a) Distributions of u-velocity along the vertical centerline of the simulation domain. (b) Distributions of u-velocity along vertical line x = 25 of the simulation domain. (c) Distributions of v-velocity along the horizontal centerline of the simulation domain. (d) Velocity U_p* that varies with time step at the grid point (25, 45).

13 shows the effects of the lattice velocity on the simulation accuracy of power law fluids. Figure 13a shows the effects of lattice velocity on the simulation accuracy of the TRT−LBM. Figure 13b shows the effects of lattice velocity on the simulation accuracy of SRT−LBM. As can be seen from Figure 13a, for TRT−LBM, with the increase in lattice velocity, the relative error increases slowly along the nonlinear curve. The fitting functions corresponding to n = 0.5, 1, and 1.5 are $\mathrm{Err}(U^*) = 64.74U^{1.98}$, $\mathrm{Err}(U^*) = 150.2U^{2.024}$, and $\mathrm{Err}(U^*) = 5058.97U^{2.48}$, respectively. As shown in Figure 13b, for SRT−LBM, with an increase of lattice velocity, the relative error increases sharply. By comparing Figure 13a,b, it can be found that the accuracy of TRT−LBM is much higher than that of SRT−LBM.

As shown in Figures 7−13, lattice velocity U has considerable effects on the stability and convergence rate of the simulation. As can be seen from Figures 7, 9, 11, and 13a, for the TRT−LBM, the lattice velocity, U, has a slight effect on the simulation accuracy but notable effects on the convergence rates. In a certain range, the larger the lattice velocity is, the faster the convergence rate. As shown in Figures 8, 10, 12, and 13b, for the SRT−LBM, the lattice velocity, U, has pronounced effects on simulation accuracy and convergence rates. In a certain range, the larger the lattice velocity U, the faster the convergence rate but the lower the simulation accuracy. By comparing Figures 7 and 8, 9 and 10, 11 and 12, and 13a,b, it can be observed that the TRT model can select the lattice velocity, U, in a larger range to improve the convergence rate and retain the accuracy basically unchanged. However, the accuracy of the SRT model is closely related to the lattice velocity, U, and the larger the lattice velocity, the lower the accuracy.

As can be seen from Figures 7, 8, and 13, for the TRT−LBM, when n = 0.5 and lattice velocity U = 0.002, it takes 5720 time steps to converge, and the relative error is 0.000269. When lattice velocity U = 0.008, it only takes 1880 time steps to converge; the relative error is 0.00447. However, for the SRT−LBM, when lattice velocity U = 0.001, it takes 8680 time steps to converge; the relative error is 0.01377. When lattice velocity U = 0.002, it takes 6840 time steps to converge; the relative error is 0.01281. When lattice velocity U = 0.004, it takes 4400 time steps to converge; the relative error is 0.03176. Therefore, when n = 0.5, the time step required by the SRT−LBM is approximately 3−5 times that of the TRT−LBM for meeting the accuracy requirements.

As shown in Figures 9, 10, and 13, for the TRT−LBM, when n = 1 and lattice velocity U = 0.008, it only takes 1560 time steps to converge; the relative error is 0.00858. However, for

https://doi.org/10.1021/acsomega.3c06663
ACS Omega 2023, 8, 47991−48018

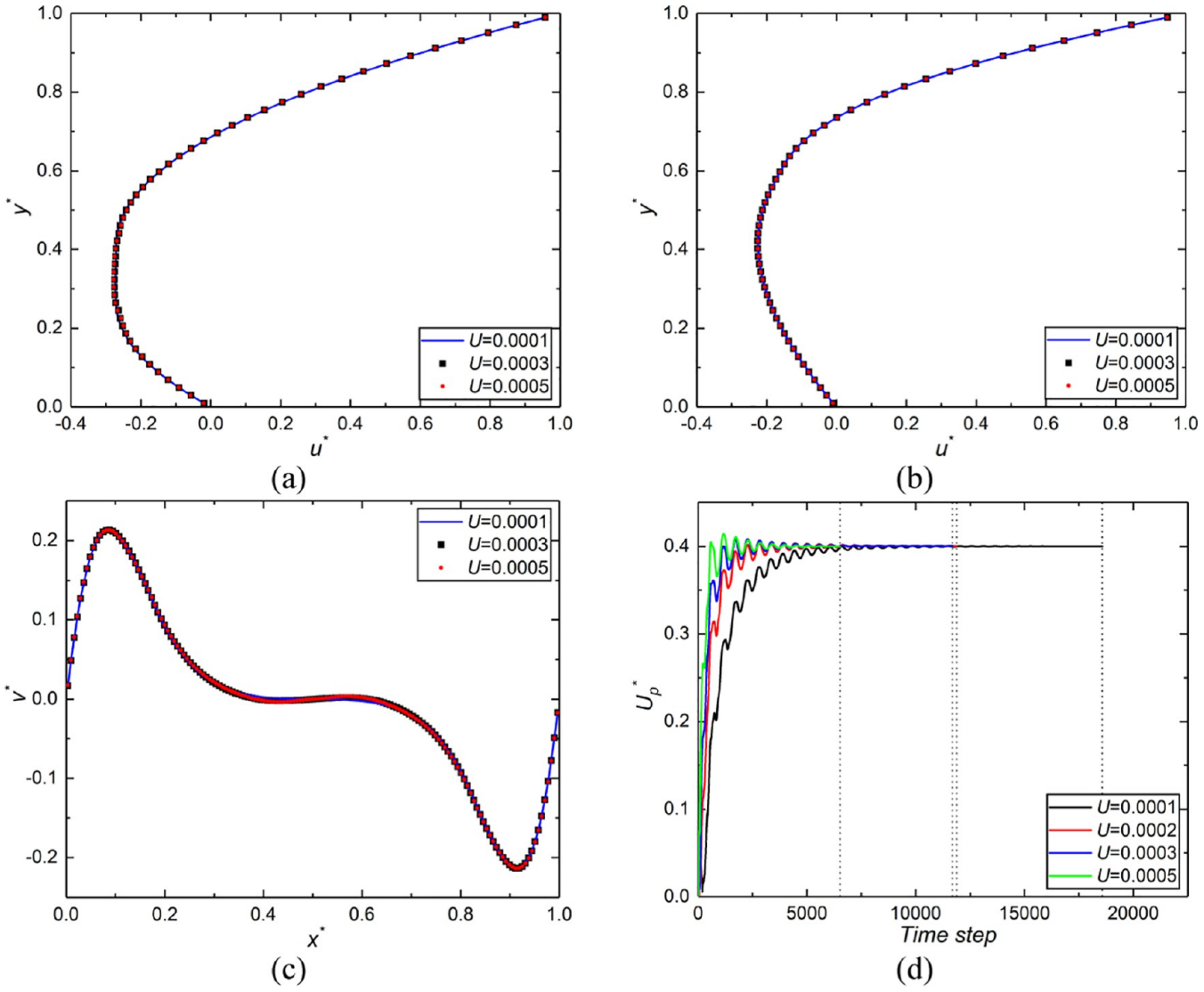

Figure 15. Simulation results of the SRT−LBM for Bingham fluids at Bn = 0.5 (Re_B = 0.144). (a) Distributions of u-velocity along the vertical centerline of the simulation domain. (b) Distributions of u-velocity along vertical line x = 25 of the simulation domain. (c) Distributions of v-velocity along the horizontal centerline of the simulation domain. (d) Velocity U_p* that varies with time step at the grid point (25, 45).

the SRT−LBM, when lattice velocity U = 0.0005, it takes 11,280 time steps to converge; the relative error is 0.0031. When lattice velocity U = 0.001, it takes 6400 time steps to converge, and the relative error is 0.01659. When lattice velocity $U \geq 0.003$, the relative error is greater than or equal to 0.07172, and the accuracy is considerably decreased. Therefore, when n = 1, the time step required by the SRT−LBM is approximately 4−6 times that of the TRT−LBM for meeting the accuracy requirements.

As can be seen from Figures 11−13, for the TRT−LBM, when n = 1.5 and lattice velocity U = 0.004, it only takes 1840 time steps to converge, and the relative error is 0.00585. However, for the SRT−LBM, when lattice velocity U = 0.0005, it takes 4720 time steps to converge, and the relative error is 0.03786. When lattice velocity U = 0.001, it takes 3960 time steps to converge, the relative error is 0.06732, and the accuracy is considerably decreased. When lattice velocity $U \geq$ 0.002, the relative error is greater than or equal to 0.11683, the simulation accuracy is considerably decreased, and the simulation process is unstable. Therefore, when n = 1.5, the time step required by the SRT−LBM is approximately 2−3 times that of the TRT−LBM for meeting the accuracy requirements.

Relaxation time τ has notable effects on the accuracy and stability of the LBM. According to eqs 9, 18, and 27, τ is dependent on the apparent viscosity of the fluid. The SRT−LBM has only one relaxation time τ, and the sufficient condition for the simulation process to be stable is relaxation time $\tau > 1/2$.[57,58] The relaxation time cannot be much greater than 1; otherwise, the simulation accuracy will be decreased.[39,42] Relaxation time τ is generally selected around 1 but cannot be close to 0.5.

For the flow of high-viscosity fluids, the Reynolds number is generally very small. To avoid relaxation time $\tau \gg 1$, lattice velocity U must be very small; otherwise, the accuracy will be considerably decreased. However, when the lattice velocity U is very small, the SRT−LBM requires a large number of time steps to converge. Therefore, when the Reynolds number is very small, SRT−LBM requires a large amount of computational time to converge.

The apparent viscosity of non-Newtonian fluids is closely related to the shear rate. Therefore, there is a large difference

https://doi.org/10.1021/acsomega.3c06663
ACS Omega 2023, 8, 47991−48018

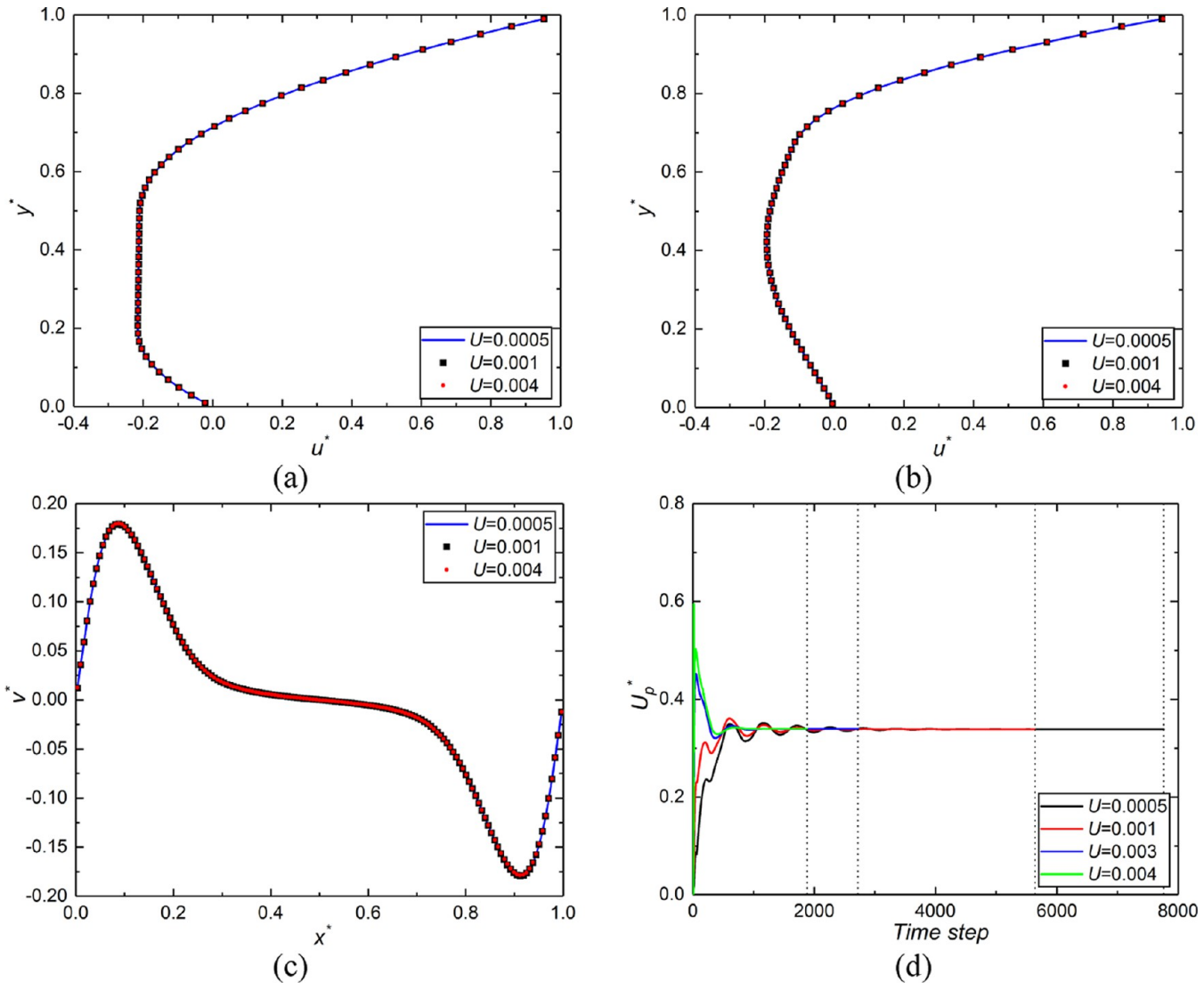

Figure 16. Simulation results of the TRT−LBM for Bingham fluids at Bn = 1.5 (Re_B = 0.144). (a) Distributions of u-velocity along the vertical centerline of the simulation domain. (b) Distributions of u-velocity along vertical line x = 25 of the simulation domain. (c) Distributions of v-velocity along the horizontal centerline of the simulation domain. (d) Velocity U_p* that varies with time step at the grid point (25, 45).

in the apparent viscosity at each grid point in the fluid domain. The relaxation time, τ, of each grid point in the simulation domain is different. When the τ value of some grid points in the computational domain approaches 0.5, the simulation process becomes unstable; however, when the τ value of some grid points in the computational domain is much greater than 1, the simulation accuracy will be considerably decreased.

The TRT−LBM has two relaxation times: τ^+ and τ^-. According to eq 18, τ^+ is related to the apparent viscosity of the fluid and τ^- is a free parameter. Equation 19 shows that τ^+ and τ^- are linked together by the magic parameter, Λ.[42] When the viscosity of the fluid changes, τ^+ changes accordingly. As long as the magic parameter Λ remains fixed, by adjustment of τ^-, the stability and accuracy of the simulation remain basically unchanged.

4.2.3. Flow of Bingham Fluids in the Cross Section of the Screw Channel. The results of the TRT and SRT models when the Bingham numbers Bn = 0.5, 1.5, and 2.5 are shown in Figures 14 and 15, 16 and 17, and 18 and 19, respectively. The distributions of u-velocity along the vertical centerline of the simulation domain are shown in Figures 14a−19a, and those along vertical line x = 25 of the simulation domain are shown in Figures 14b−19b. Similarly, the distributions of v-velocity along the horizontal centerline of the simulation domain are shown in Figures 14c−19c, and the velocity, U_p*, that varies with time step at the grid point (25, 45) are shown in Figures 14d−19d. The flow field is steady state. The variation of velocity U_p* with the time step is the numerical value generated by the LBM model algorithm during the iteration process.

To compare the accuracy of TRT−LBM and SRT−LBM in simulating Bingham fluids, we used eq 43 to calculate the relative errors at different lattice velocities. Since there is no analytical solution, we take the numerical results of TRT−LBM corresponding to lattice velocity U = 0.0005 as reference solution U_r*(x,y) because, in general, the smaller the lattice velocity, the higher the simulation accuracy. Figure 20 shows the effects of the lattice velocity on the simulation accuracy of Bingham fluids. Figure 20a shows the effects of lattice velocity on the simulation accuracy of the TRT−LBM. Figure 20b shows the effects of lattice velocity on the simulation accuracy of SRT−LBM. As can be seen from Figure 20a, for TRT−

https://doi.org/10.1021/acsomega.3c06663
ACS Omega 2023, 8, 47991−48018

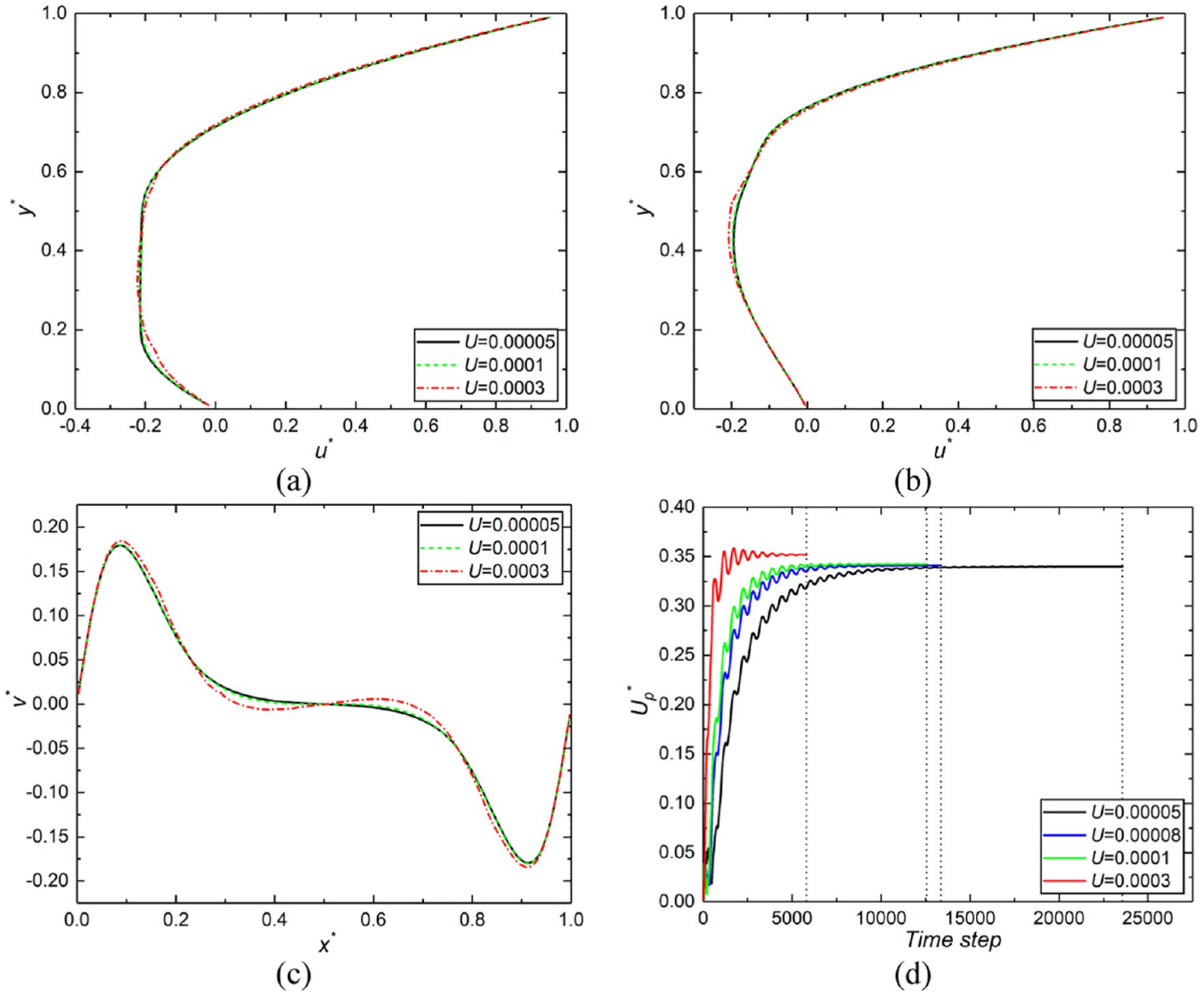

Figure 17. Simulation results of the SRT−LBM for Bingham fluids at Bn = 1.5 (Re_B = 0.144). (a) Distributions of u-velocity along the vertical centerline of the simulation domain. (b) Distributions of u-velocity along vertical line x = 25 of the simulation domain. (c) Distributions of v-velocity along the horizontal centerline of the simulation domain. (d) Velocity U_p* that varies with time step at the grid point (25, 45).

LBM, with the increase in lattice velocity, the relative error increases slowly along the nonlinear curve. As shown in Figure 20b, for SRT−LBM, when Bn = 0.5, with the increase of lattice velocity, the relative error first decreases slowly and then increases slowly. The SRT−LBM can obtain high-accuracy results when Bn = 0.5. However, when Bn = 1.5 and 2.5, with the increase of lattice velocity, the relative error first decreases sharply and then increases sharply. When Bn = 1.5 and 2.5, the SRT−LBM is difficult to obtain high-accuracy results. By comparing Figure 20a,b, it can be found that the accuracy of the TRT−LBM is much higher than that of the SRT−LBM.

As shown in Figures 14, 15, and 20, for the TRT−LBM, when Bingham number Bn = 0.5 and lattice velocity U = 0.002, it takes 4160 time steps to converge, and the relative error is 0.0006097. When lattice velocity U = 0.006, it only takes 1760 time steps to converge; the relative error is 0.00577. However, for the SRT−LBM, when lattice velocity U = 0.0001, it takes 18,560 time steps to converge, and the relative error is 0.01177. When lattice velocity U = 0.0003, it takes 11,680 time steps to converge, and the relative error is 0.00621. When lattice velocity U = 0.0005, it takes 6520 time steps to converge, the relative error is 0.0089, and the simulation process is unstable. Therefore, when Bingham number Bn = 0.5, the time step required by the SRT−LBM is approximately 6−7 times that required by the TRT−LBM for meeting the accuracy requirements.

As can be seen from Figures 16, 17, and 20, for the TRT−LBM, when Bingham number Bn = 1.5 and lattice velocity U = 0.002, it takes 3480 time steps to converge, and the relative error is 0.0008166. When lattice velocity U = 0.004, it only takes 1880 time steps to converge, and the relative error is 0.00339. However, for the SRT−LBM, when lattice velocity U = 0.00008, it takes 13,360 time steps to converge; the relative error is 0.01614. When lattice velocity U = 0.0001, it takes 12,560 time steps to converge, the relative error is 0.01511. When lattice velocity U = 0.0003, it takes 5800 time steps to converge, and the relative error is 0.02987. When lattice velocity U = 0.0005, it takes 6440 time steps to converge, and the relative error is 0.03839. Therefore, when Bingham number Bn = 1.5, the time step required by the SRT−LBM is

https://doi.org/10.1021/acsomega.3c06663
ACS Omega 2023, 8, 47991−48018

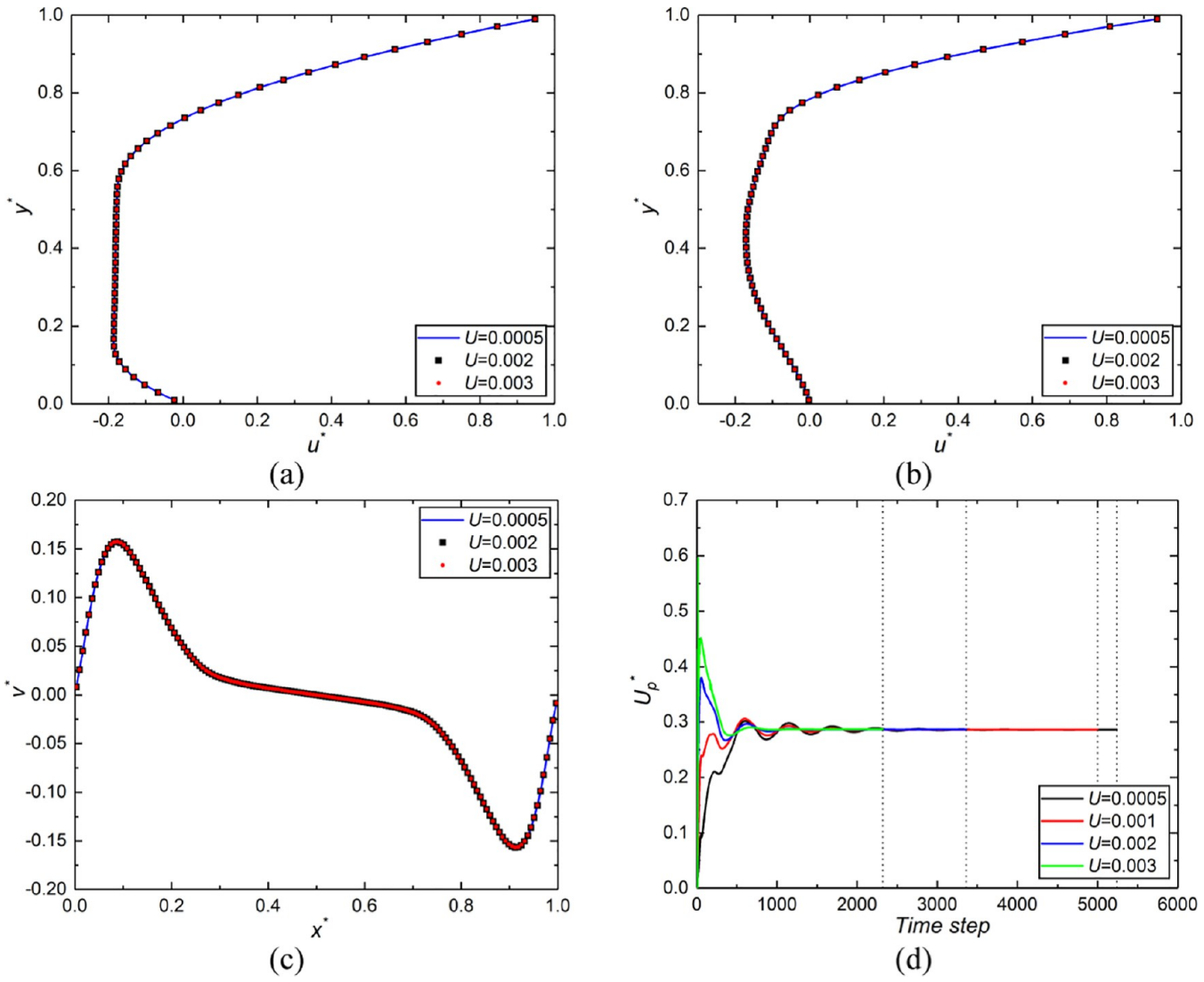

Figure 18. Simulation results of the TRT−LBM for Bingham fluids at Bn = 2.5 (Re_B = 0.144). (a) Distributions of u-velocity along the vertical centerline of the simulation domain. (b) Distributions of u-velocity along vertical line x = 25 of the simulation domain. (c) Distributions of v-velocity along the horizontal centerline of the simulation domain. (d) Velocity U_p* that varies with time step at the grid point (25, 45).

approximately 6−7 times that of the TRT−LBM for meeting the accuracy requirements. The accuracy of the TRT−LBM is significantly higher than that of the SRT−LBM.

As can be seen from Figures 18, 19, and 20, for the TRT−LBM, when Bingham number Bn = 2.5 and lattice velocity U = 0.001, it takes 5000 time steps to converge, and the relative error is 0.0004373. When lattice velocity U = 0.003, it takes only 2320 time steps to converge, and the relative error is 0.0024. However, for the SRT−LBM, when lattice velocity U = 0.00006, it takes 15,480 time steps to converge, the relative error is 0.0209, and the simulation process is unstable. When lattice velocity U = 0.0001, it takes 8720 time steps to converge, the relative error is 0.02046, and the simulation process is unstable. When lattice velocity U = 0.0003, it takes 7320 time steps to converge, the relative error is 0.05339, and the simulation process is very unstable and divergence. Therefore, when Bingham number Bn = 2.5, the TRT−LBM can simulate efficiently, stably, and accurately. However, the SRT−LBM is inaccurate and unstable, and the computational efficiency is very low.

Many materials, such as Bingham fluids, Casson fluids, and Herschel−Bulkley fluids, have yield stress. When the shear rate of the local area in the simulation domain is very small, the apparent viscosity of the local area will be very large; the relaxation time of the local area may be much greater than 1, and the simulation accuracy is considerably decreased. According to eq 41, when Re_B and Bn are constant, the apparent viscosity and yield stress can be reduced by reducing the lattice velocity so that the relaxation time is within a reasonable range. Therefore, for the SRT−LBM, when the lattice velocity is very small, we can obtain accurate results. As shown in Figures 15, 17, and 19, for the SRT−LBM, the larger the Bingham number, the smaller the lattice velocity must be, the more unstable the simulation process, and the more time steps required.

For fluids with yield stress, the apparent viscosity of the local area in the simulation domain may be very large, resulting in relaxation time $\tau^+ \gg 1$. The TRT−LBM can overcome these difficulties effectively. For the TRT−LBM, as long as the relaxation time, τ^-, of each grid point in the simulation domain is adjusted to maintain the magic parameter, Λ, of each grid

https://doi.org/10.1021/acsomega.3c06663
ACS Omega 2023, 8, 47991−48018

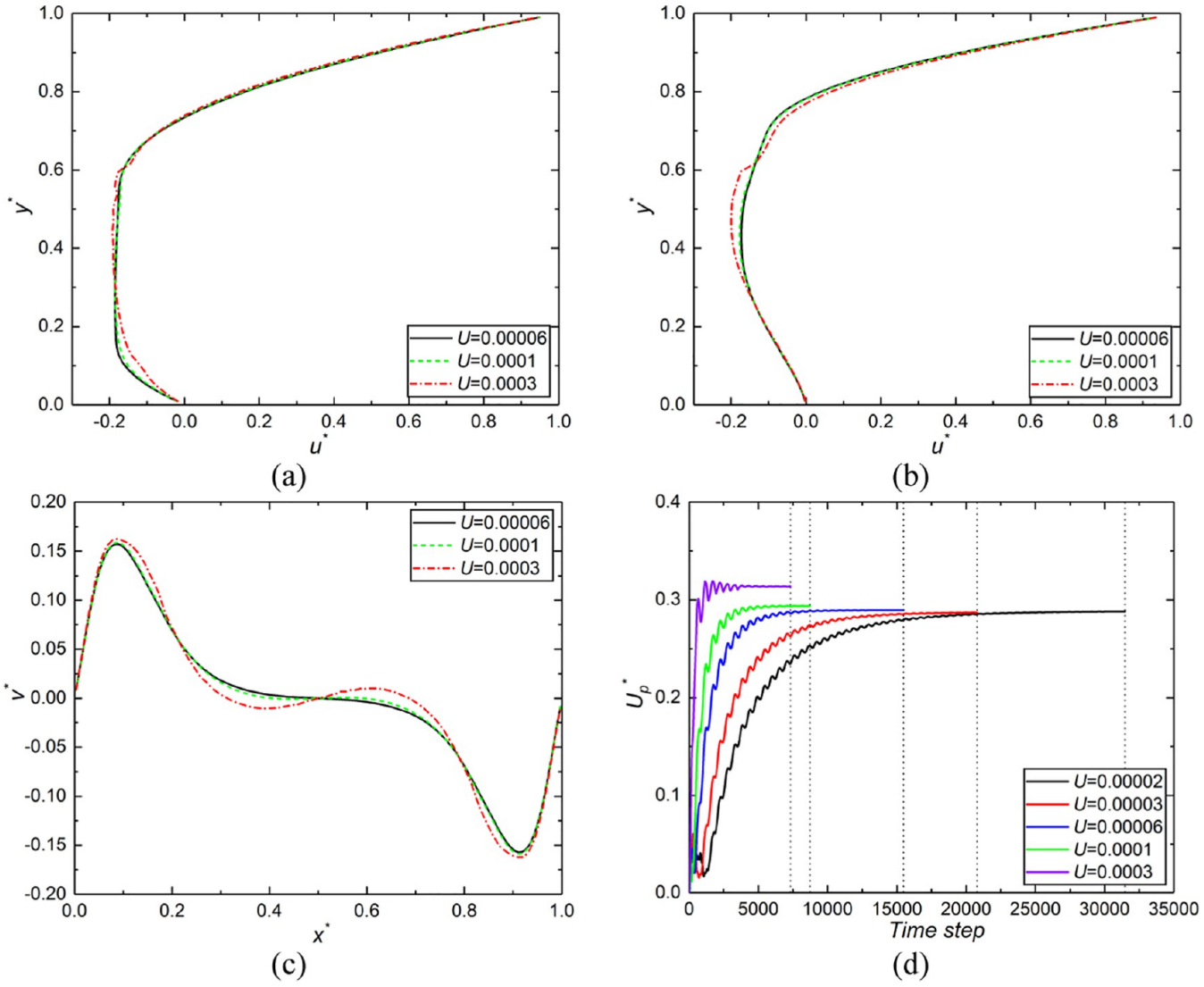

Figure 19. Simulation results of the SRT−LBM for Bingham fluids at Bn = 2.5 (Re_B = 0.144). (a) Distributions of u-velocity along the vertical centerline of the simulation domain. (b) Distributions of u-velocity along vertical line x = 25 of the simulation domain. (c) Distributions of v-velocity along the horizontal centerline of the simulation domain. (d) Velocity U_p* that varies with time step at the grid point (25, 45).

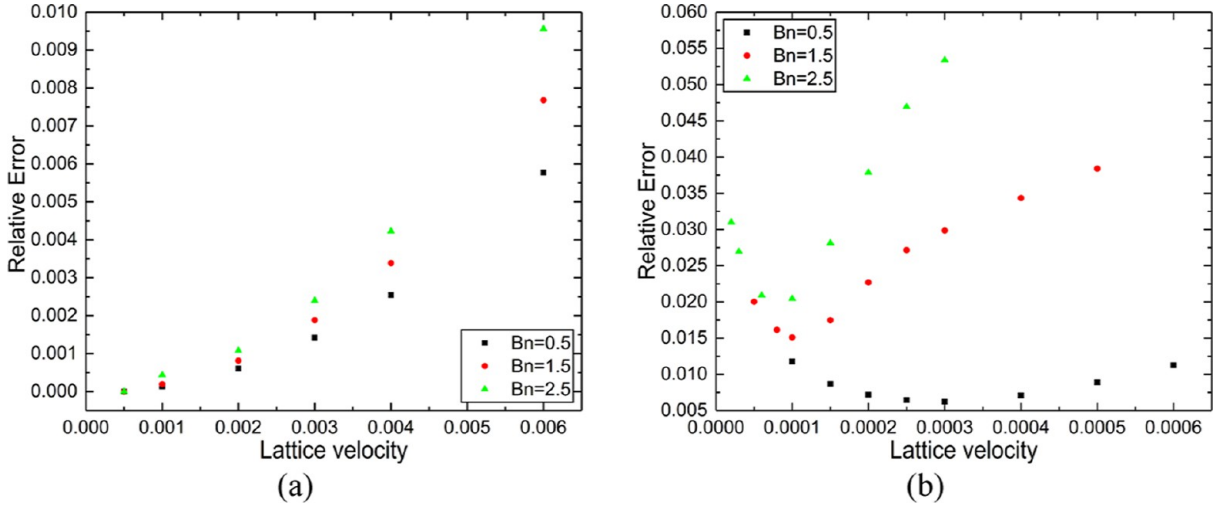

Figure 20. Effects of lattice velocity U on simulation accuracy of Bingham fluids. (a) Simulation accuracy of TRT−LBM. (b) Simulation accuracy of SRT−LBM.

https://doi.org/10.1021/acsomega.3c06663
ACS Omega 2023, 8, 47991−48018

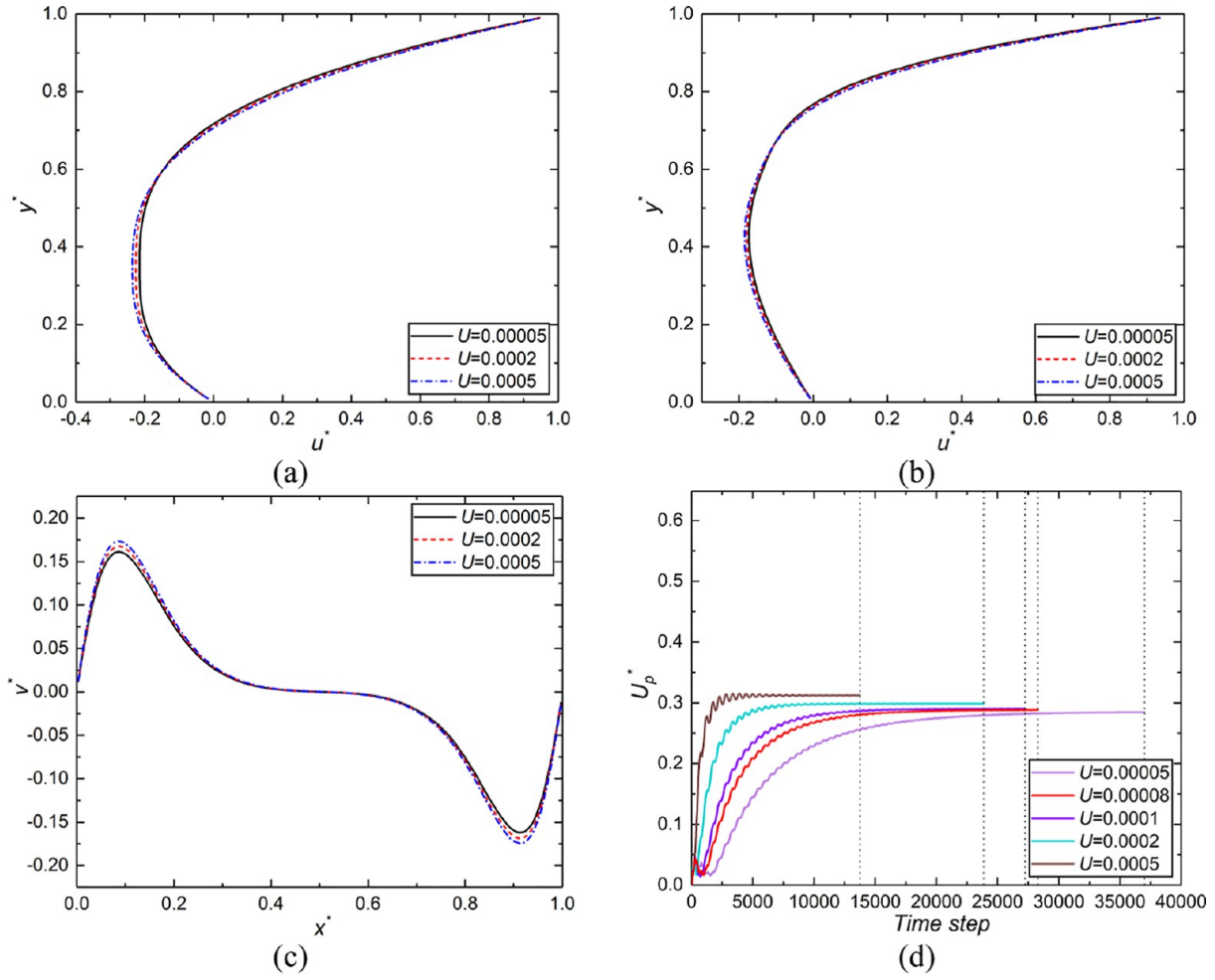

Figure 21. Simulation results of the MRT−LBM for power law fluids at n = 0.5 (Re_p = 0.144). (a) Distributions of u-velocity along the vertical centerline of the simulation domain. (b) Distributions of u-velocity along vertical line x = 25 of the simulation domain. (c) Distributions of v-velocity along the horizontal centerline of the simulation domain. (d) Velocity U_p* that varies with time step at the grid point (25, 45).

point fixed, the simulation process can be stable, and high-accuracy results can be obtained. Moreover, the relaxation time, τ^+, should be increased within a certain range; if τ^+ is too large, the simulation accuracy will decrease.

4.3. Effectiveness of the MRT−LBM for High-Viscosity Power Law Fluids. The MRT−LBM has multiple relaxation parameters, and its stability is better than that of SRT−LBM, especially for high Reynolds number problems. To the best of our knowledge, few people have used the MRT−LBM to study generalized Newtonian fluids with high viscosities. To verify the effectiveness of the MRT model in simulating high-viscosity generalized Newtonian fluids, we used the MRT−LBM to study the flow field of power law fluids in the cross section of the screw channel. The diagonal relaxation matrix S has considerable effects on the stability and accuracy of simulation. The relaxation parameters of the MRT model selected in this paper are optimized by other researchers for non-Newtonian fluids. When the MRT model is used to study non-Newtonian fluids, many researchers use the same set of relaxation parameters.[33−37] This set of relaxation parameters is S = diag(0, 1.1, 1.0, 0, 1.2, 0, 1.2, 1/τ, 1/τ). These relaxation parameters were selected by predecessors based on Lallemand and Luo[12] and are not the optimal parameters obtained by mathematical analysis. These relaxation parameters have been verified by predecessors and are suitable for non-Newtonian fluids, but they are not necessarily the optimal parameters. At present, the optimal relaxation parameters suitable for non-Newtonian fluids have not been obtained. Herein, we attempted to use other relaxation parameters, but the effect was not notable.

The simulation results of the MRT−LBM when power law index n = 0.5, 1, and 1.5 are shown in Figures 21, 22, and 23, respectively. The distributions of u-velocity along the vertical centerline of the simulation domain are shown in Figures 21a−23a, and those along vertical line x = 25 of the simulation domain are shown in Figures 21b−23b. Similarly, the distributions of v-velocity along the horizontal centerline of the simulation domain are shown in Figures 21c−23c, and velocity U_p* that varies with time step at the grid point (25, 45) is shown in Figures 21d−23d. The flow field is steady state. The variation of velocity U_p* with the time step is the numerical value generated by the LBM model algorithm during the iteration process.

Figure 24 shows the effects of lattice velocity on the accuracy of the MRT−LBM in simulating power law fluids. As can be seen from Figure 24, when n = 1, with the increase of lattice velocity, the relative error increases slowly. However, when n = 0.5 and 1.5, with the increase of lattice velocity, the relative error increases sharply; only when the lattice velocity is very

https://doi.org/10.1021/acsomega.3c06663
ACS Omega 2023, 8, 47991−48018

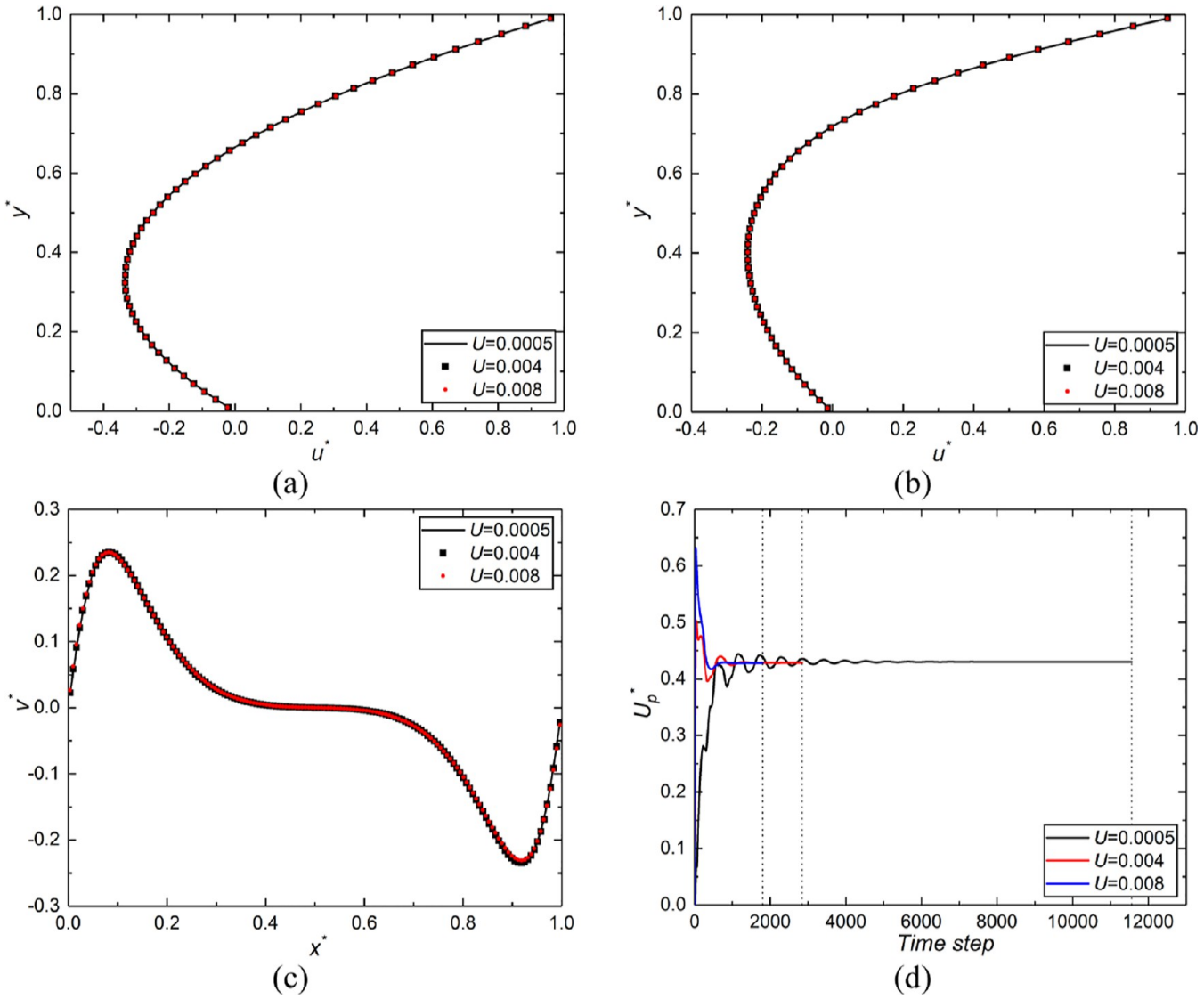

Figure 22. Simulation results of the MRT−LBM for power law fluids at n = 1 (Re_p = 0.144). (a) Distributions of u-velocity along the vertical centerline of the simulation domain. (b) Distributions of u-velocity along vertical line x = 25 of the simulation domain. (c) Distributions of v-velocity along the horizontal centerline of the simulation domain. (d) Velocity U_p* that varies with time step at the grid point (25, 45).

small can high accuracy results be obtained, which requires a lot of computational time.

As can be seen from Figures 21 and 24, for n = 0.5, when lattice velocity U = 0.00005, it takes 37,000 time steps to converge; the relative error is 0.02918. When lattice velocity U = 0.0002, it takes 23,880 time steps to converge, and the relative error is 0.04672. When lattice velocity U = 0.0003, it takes 15,840 time steps to converge, and the relative error is 0.05666. As shown in Figures 22 and 24, for n = 1, when lattice velocity U = 0.0005, it takes 11,560 time steps to converge, and the relative error is 0.000368. When lattice velocity U = 0.002, it takes 4800 time steps to converge, the relative error is 0.01158. When lattice velocity U = 0.008, it takes 1800 time steps to converge, and the relative error is 0.03601. As can be seen from Figures 23 and 24, for n = 1.5, when lattice velocity U = 0.0001, it takes 16,520 time steps to converge; the relative error is 0.00825. When lattice velocity U = 0.0005, it takes 6880 time steps to converge, and the relative error is 0.0252. When lattice velocity U = 0.002, it takes 4560 time steps to converge, and the relative error is 0.05067. Therefore, when the Reynolds number is very small, the MRT−LBM can simulate Newtonian fluids efficiently and accurately. However, for shear-thinning fluids and shear-thickening fluids, the accuracy of the simulation results depends on the lattice velocity. Only when the lattice velocity is very small can high-accuracy results be obtained, which requires a large amount of computational time.

The MRT model contains many free parameters that can adjust accuracy and stability and is the most general model. The MRT model can be simplified to the TRT or SRT model. For the MRT model, when all even order moments are relaxed with ω^+ and all odd order moments with ω^-, and eq 19 is satisfied, the MRT model can be simplified to the TRT model. However, only by optimizing the relaxation parameters can the advantages of the MRT model be fully utilized. Unfortunately, currently, no effective method is available to optimize these relaxation parameters.[39] The optimization of the accuracy and stability of the MRT models via parameter research or linear stability analysis is difficult.

https://doi.org/10.1021/acsomega.3c06663
ACS Omega 2023, 8, 47991−48018

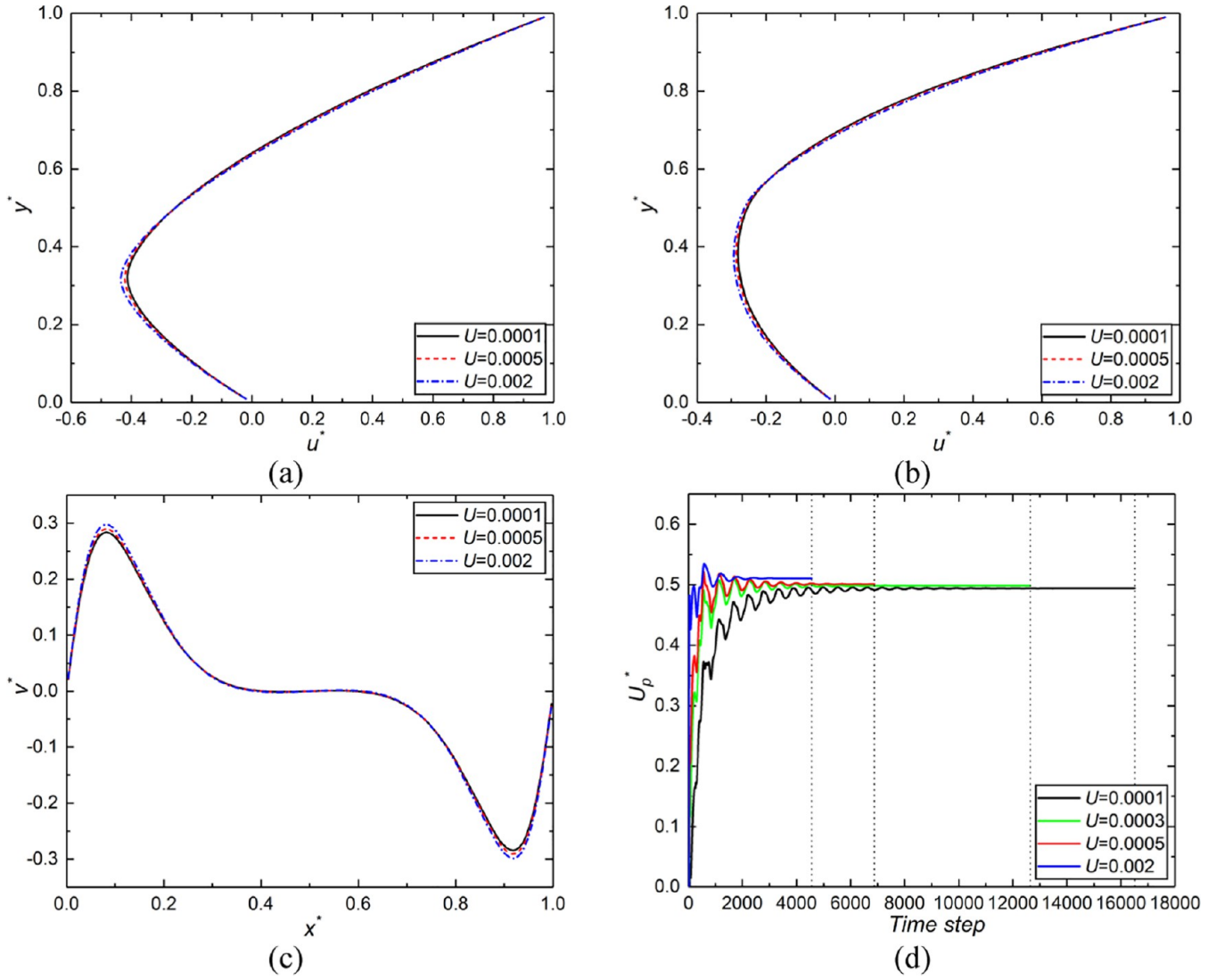

Figure 23. Simulation results of the MRT−LBM for power law fluids at n = 1.5 (Re_p = 0.144). (a) Distributions of u-velocity along the vertical centerline of the simulation domain. (b) Distributions of u-velocity along vertical line x = 25 of the simulation domain. (c) Distributions of v-velocity along the horizontal centerline of the simulation domain. (d) Velocity U_p* that varies with time step at the grid point (25, 45).

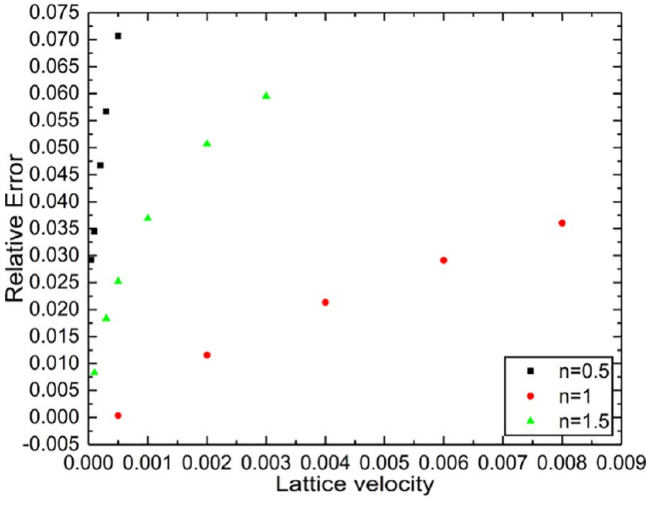

Figure 24. Effects of the lattice velocity on the accuracy of the MRT−LBM in simulating power law fluids.

For Newtonian fluids, the viscosity does not vary with the shear rate, and the relaxation time corresponding to the viscosity is fixed. First, we can simplify the MRT model to the TRT model and then adjust some free parameters separately. By reasonably fine-tuning the free parameters, the MRT model can obtain more stable and accurate results than the TRT model. However, for non-Newtonian fluids, the apparent viscosity is related to the shear rate, and the relaxation times of each grid point in the fluid domain are very different. It is difficult to make the accuracy and stability of the MRT model superior to those of the TRT model by adjusting the free parameters. For high-viscosity non-Newtonian fluids, optimizing the relaxation-time parameters of the MRT model is more difficult. In addition, although the MRT model can be simplified to the TRT model, the execution process of its program remains unchanged and requires a larger computational memory and longer computational time than the TRT model. Therefore, it is difficult for the MRT−LBM to realize its potential when simulating high-viscosity non-Newtonian fluids.

https://doi.org/10.1021/acsomega.3c06663
ACS Omega 2023, 8, 47991−48018

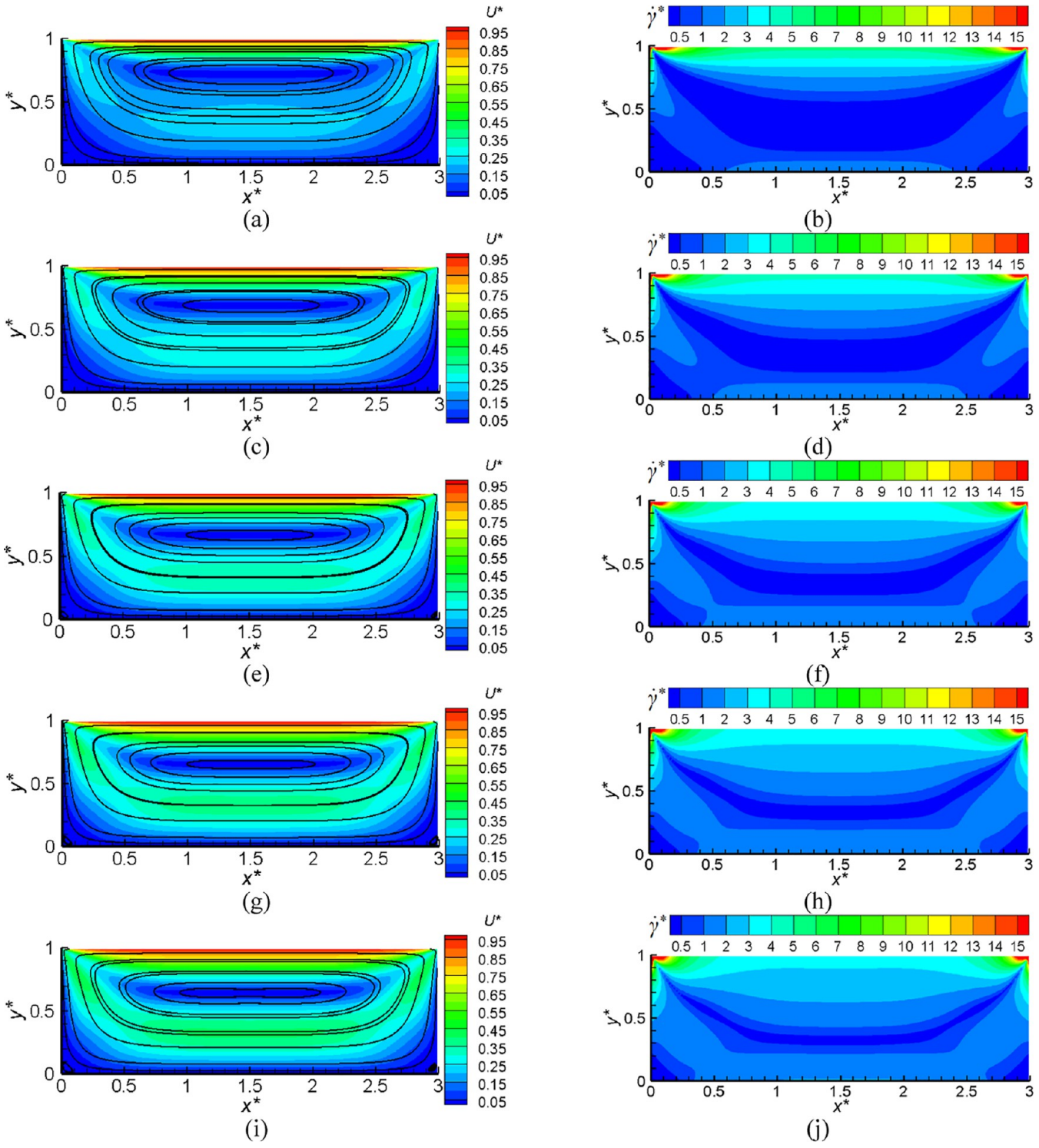

Figure 25. Flow patterns of power law fluids in the screw channel for various n values (Re_p = 0.144). (a,c,e,g,i) Velocity and streamlines at n = 0.5, 0.75, 1, 1.25, and 1.5. (b,d,f,h,j) Shear rates at n = 0.5, 0.75, 1, 1.25, and 1.5, respectively.

4.4. Flow Patterns of Generalized Newtonian Fluids in the Cross Section of the Screw Channel. *4.4.1. Flow Patterns of Power Law Fluids in the Screw Channel.* The flow patterns of power law fluids in the cross section of the screw channel are shown in Figure 25; the velocity magnitude and streamlines at n = 0.5, 0.75, 1, 1.25, and 1.5 are shown in Figure 25a,c,e,g,i, and the shear rates at n = 0.5, 0.75, 1, 1.25, and 1.5 are shown in Figure 25b,d,f,h,j, respectively.

As shown in Figure 25, power law index n has considerable effects on the flow field in a single-screw extruder. When n = 1, 1.25, and 1.5, small circulations are observed at the bottom corner of the screw channel. However, when n = 0.5 and 0.75, small circulations are not observed at the bottom corner of the screw channel. For Newtonian fluids (n = 1), both the visualization experimental results of Yao et al.[4,5] and the simulation results obtained by Horiguchi et al.[6] indicated small circulations at the bottom corner of the screw channel.

https://doi.org/10.1021/acsomega.3c06663
ACS Omega 2023, 8, 47991−48018

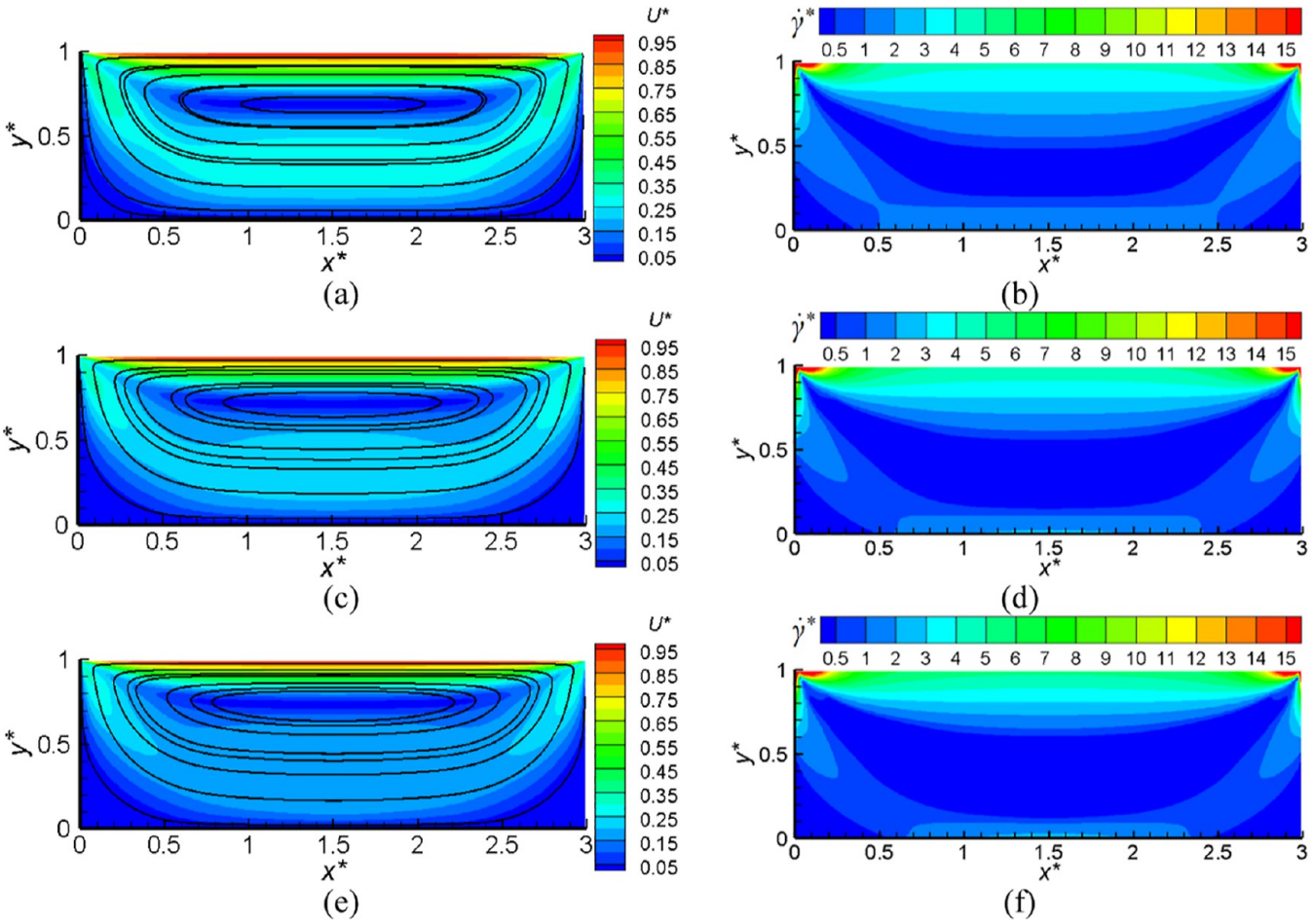

Figure 26. Flow patterns of Bingham fluids in the screw channel for various *Bn* values (Re_B = 0.144). (a,c,e) Velocity and streamlines at *Bn* = 0.5, 1.5, and 2.5. (b,d,f) Shear rates at *Bn* = 0.5, 1.5, and 2.5, respectively.

However, Buick et al.[7−9] did not observe small circulations at the bottom corner of the screw channel.

As shown in Figure 25a,c,e,g,i, the power law index has considerable effects on the velocity distribution of polymer melts. Fluid particles circulate along fixed trajectories in the cross section of the screw channel. As shown in Figure 25, in a cycle, the shear deformation of fluid particles at different positions is different. The polymer melt is a high-viscosity fluid, and its mixing process is mainly achieved via laminar shear. The magnitude and distribution of the shear rate can reflect the mixing effect of the polymer melts. As shown in Figure 25b,d,f,h,j, the mixing effect of the fluid that is located in the neighborhood of the barrel, and the screw is better than that in the middle of the channel. Under the same operating conditions, the smaller the *n*, the poorer the mixing effect of the fluid domain in the middle of the screw channel. When $n \leq 0.5$, the mixing quality of the polymer melt is poor, and the mixing quality needs to be improved by increasing the rotational speed of the screw or changing the width/height ratio of the screw channel. In addition, as shown in Figure 25b,d,f,h,j, the shear rate at the bottom corner of the screw channel is very small, and the mixing effect of the fluid is very poor. Therefore, the bottom corner of the screw should be designed as rounded corners.

4.4.2. Flow Patterns of Bingham Fluids in the Screw Channel. Figure 26 shows the flow patterns of Bingham fluids in the cross section of the screw channel. The velocity magnitude and streamlines at *Bn* = 0.5, 1.5, and 2.5 and the shear rates at *Bn* = 0.5, 1.5, and 2.5 are shown in Figures 26a,c,e and 26b,d,f, respectively. As shown in Figure 26, the Bingham number has notable effects on the velocity distribution and shear rate distribution. Fluid particles circulate along fixed trajectories in the screw channel. As shown in Figure 26a,c,e, for Bingham fluids, small circulations are not observed at the bottom corner of the screw channel. As shown in Figure 26b,d,f, the mixing effect of the fluid that is located in the neighborhood of the barrel and the screw is better than that in the middle of the channel. Under the same operating conditions, the larger the Bingham number, the poorer the mixing effect of the fluid domain in the middle of the screw channel. Therefore, the mixing quality needs to be improved by increasing the rotational speed of the screw or changing the width/height ratio of the screw channel. In addition, as shown in Figure 26b,d,f, the shear rate at the bottom corner of the screw is very small, and the mixing effect of the fluid is very poor. Therefore, the bottom corner of the screw should be designed as rounded corners.

4.5. Flow Patterns of Generalized Newtonian Fluids in the Pin Mixing Screw. Yao et al.[4,5] have studied the flow of fluids in the pin mixing screw by visualization experiments. In their experiment, the width, *W*, and height, *H*, of the rectangular cavity are 0.225 and 0.066 m, respectively, and the width, *w*, and height, *h*, of the pins are 0.0231 and 0.0479 m, respectively. The fluid used in the experiment is corn syrup.

https://doi.org/10.1021/acsomega.3c06663
ACS Omega 2023, 8, 47991−48018

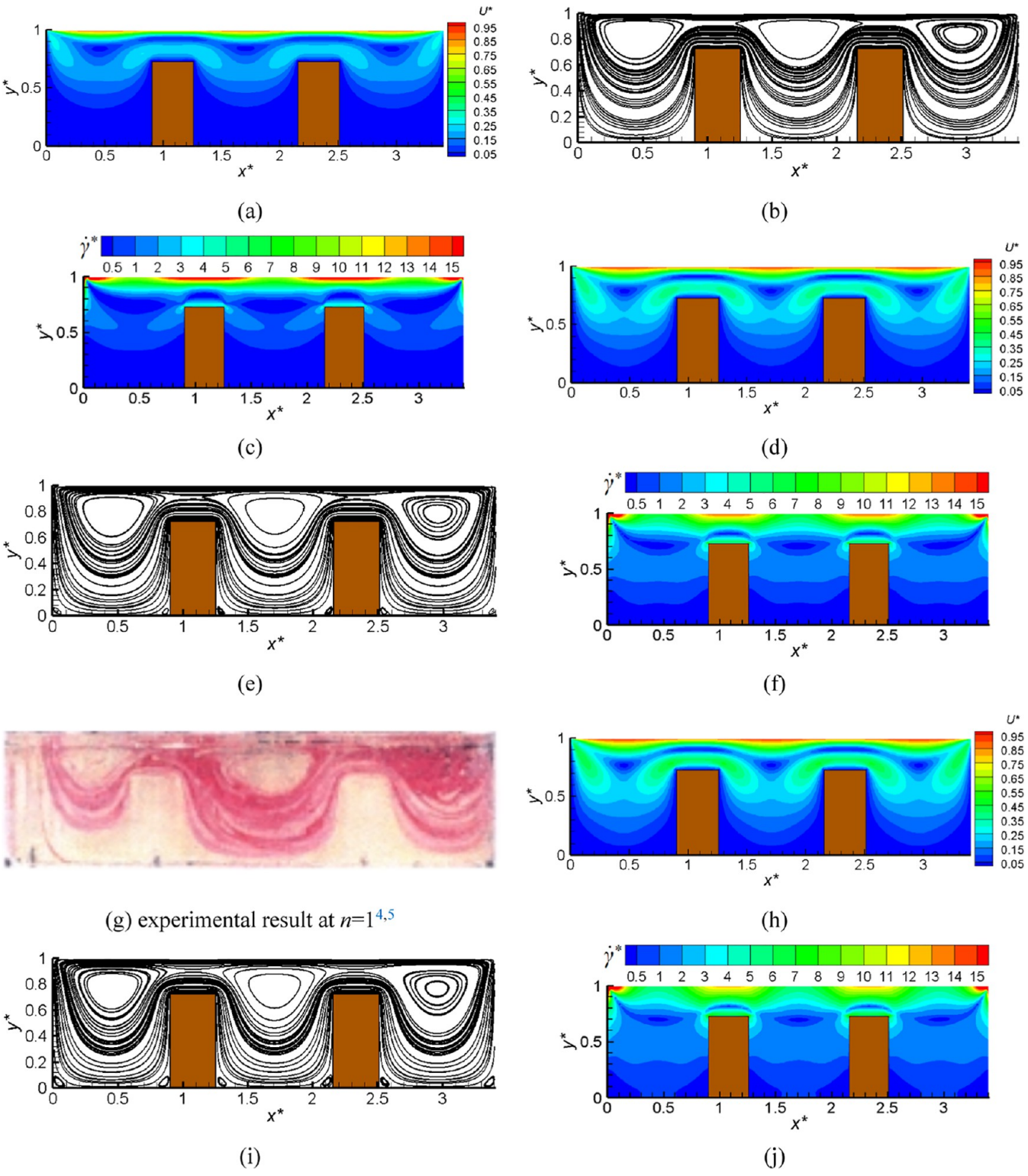

Figure 27. Flow patterns of power law fluids in the pin mixing screw for various n values (Re_p = 0.054). (a,d,h) Velocity magnitude at n = 0.5, 1, and 1.5; (b,e,i) streamlines at n = 0.5, 1, and 1.5; and (c,f,j) shear rates at n = 0.5, 1, and 1.5, respectively. (g) Experimental result at n = 1[4,5]

The viscosity of the corn syrup is 12 Pa s, and the density of the corn syrup is 1.4×10^3 kg/m^3. The speed of the drive belt is 0.007 m/s. Based on the experimental parameters of Yao et al.,[4,5] we divided the simulation domain into 174 × 51 grid points in x and y directions, respectively. The pin is divided into 38 × 18 grid points. According to eq 40, Re_p = 0.054. The Reynolds number (Re_p, Re_B) is fixed at 0.054.

4.5.1. Flow Patterns of Power Law Fluids in the Pin Mixing Screw. Figure 27 shows the flow patterns of power law fluids in the cross section of a pin mixing screw. The velocity magnitude at n = 0.5, 1, and 1.5 and the streamlines at n = 0.5, 1, and 1.5 are shown in Figure 27a,d,h and 27b,e,i, respectively. Figure 27g shows the experimental result at n = 1. The shear rates at n = 0.5, 1, and 1.5 are shown in Figure 27c,f,j.

https://doi.org/10.1021/acsomega.3c06663
ACS Omega 2023, 8, 47991−48018

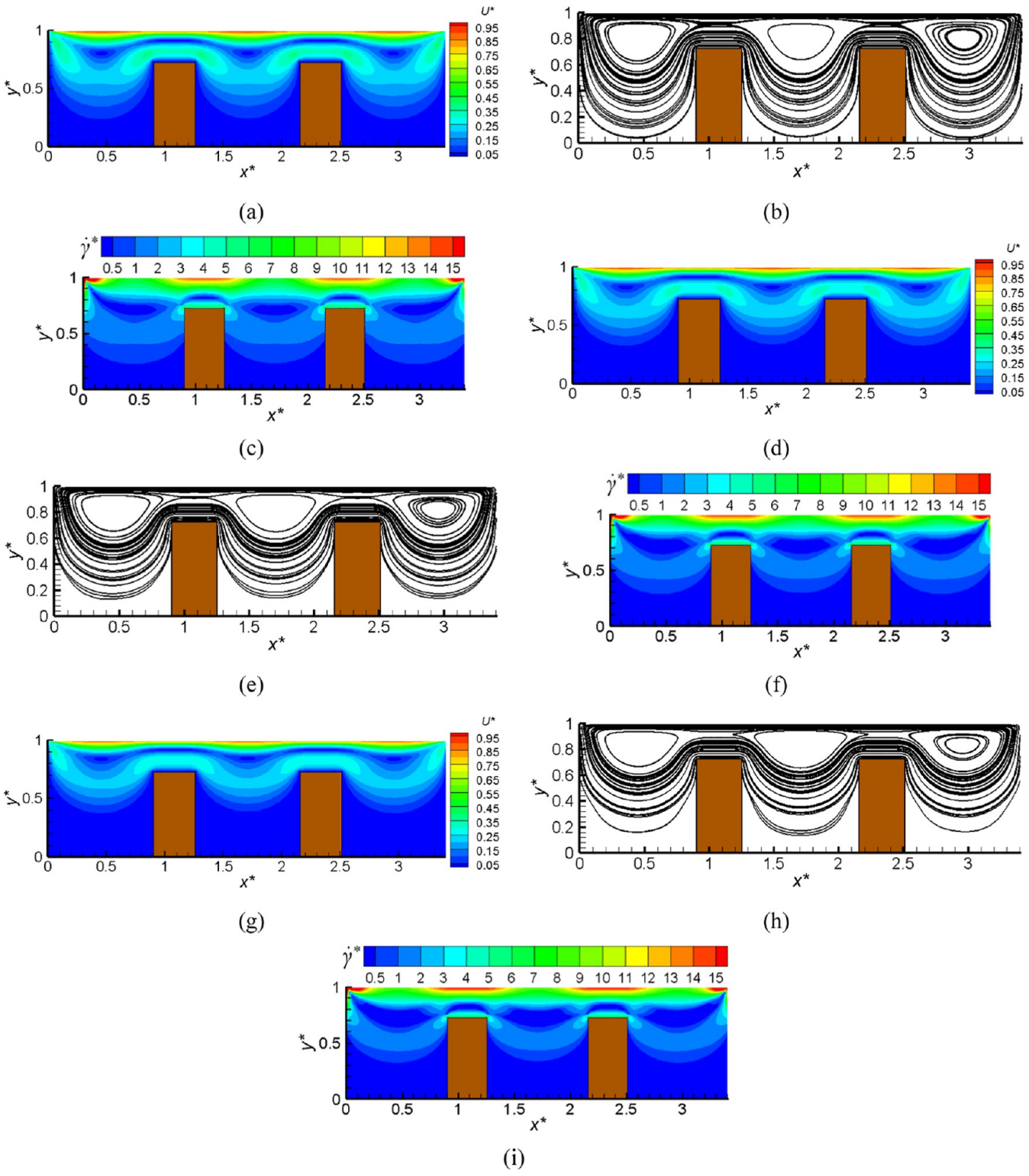

Figure 28. Flow patterns of Bingham fluids in the pin mixing screw for various *Bn* values (Re_B = 0.054). (a,d,g) Velocity magnitude at *Bn* = 0.5, 1.5, and 2.5; (b,e,h) streamlines at *Bn* = 0.5, 1.5, and 2.5; and (c,f,i) shear rates at *Bn* = 0.5, 1.5, and 2.5.

As shown in Figure 27, the power law index, *n*, has considerable effects on the velocity and shear rate distributions of polymer melts. As shown in Figure 27b,e,i, when *n* = 1 and 1.5, small circulations are observed at the bottom corner of the screw channel. However, when *n* = 0.5, small circulations are not observed at the bottom corner of the screw channel. As shown in Figure 27e,g, the numerical results by the TRT−LBM agree well with the visualization experimental results of Yao et al.[4,5] As shown in Figure 27c,f,j, the smaller the *n*, the poorer the mixing effect. When *n* = 0.5, the mixing effect is poor. The mixing quality can be improved by increasing the rotational speed of the screw, changing the width/height ratio of the screw channel, or changing the geometric parameters and distribution form of the pins. As shown in Figure 27c,f,j,

https://doi.org/10.1021/acsomega.3c06663
ACS Omega 2023, 8, 47991−48018

the shear rates at the bottom corner of the screw channel and the root of the pins are very small, and the mixing effect of the fluid is poor. Therefore, the bottom corners of the screw channel and the root of the pins should be designed as rounded corners. For the conventional extrusion screw, the fluid particles move along a helical trajectory in the screw channel. Fluid particles move along fixed shells and cannot migrate into other shells. For the pin mixing screw, the pins are evenly distributed along the down channel of the screw, causing the polymer melts to afford chaotic mixing and thus improving the mixing effect.

4.5.2. Flow Patterns of Bingham Fluids in the Pin Mixing Screw. Figure 28 shows the flow patterns of Bingham fluids in the cross section of the pin mixing screw. The velocity magnitudes at Bn = 0.5, 1.5, and 2.5; the streamlines at Bn = 0.5, 1.5, and 2.5; and the shear rates at Bn = 0.5, 1.5, and 2.5 are shown in Figure 28a,d,g; 28b,e,h; and 28c,f,i, respectively. As shown in Figure 28, the Bingham number has considerable effects on the velocity and shear rate distributions. As shown in Figure 28b,e,h, for Bingham fluids, small circulations are not observed at the bottom corner of the screw channel. However, as shown in Figure 28c,f,i, for Bingham fluids, the mixing effect is poor; the larger the Bingham number, the poorer the mixing effect. The mixing quality can be improved by increasing the rotational speed of the screw, changing the width/height ratio of the screw channel, or changing the geometric parameters and distribution form of the pins.

5. CONCLUSIONS

The SRT−LBM, TRT−LBM, and MRT−LBM have been used to study the flow field of high-viscosity generalized Newtonian fluids in the cross section of the screw channel. The stability, calculation accuracy, and calculation efficiency of SRT−LBM, TRT−LBM, and MRT−LBM have been compared in detail. The flow patterns in the cross section of a standard extrusion screw channel and an extrusion screw channel with pins were studied and compared with previous studies. The effects of the non-Newtonian properties of the fluid on the flow patterns and mixing quality have been studied. The conclusions are as follows:

1. The calculation accuracy of the SRT−LBM is heavily dependent on simulation parameters when simulating high-viscosity power law fluids. Only when the lattice velocity is very small can the accurate result be obtained, which requires a large amount of computation time. The SRT−LBM has low computational efficiency and is prone to instability when simulating high-viscosity Bingham fluids.
2. The TRT−LBM is efficient, stable, and accurate when simulating high-viscosity power law fluids and Bingham fluids. The TRT−LBM can flexibly select simulation parameters while maintaining high accuracy and can efficiently simulate fluids with yield stress, such as Bingham fluids, Casson fluids, and Herschel−Bulkley fluids.
3. The MRT−LBM can simulate high-viscosity Newtonian fluids efficiently and accurately. However, for the high-viscosity shear-thinning fluids and shear-thickening fluids, the accuracy of simulation results depends on the lattice velocity. Only when the lattice velocity is very small, can high-accuracy results be obtained, which requires a large amount of computational time.
4. The non-Newtonian properties of polymer melts have considerable effects on the flow patterns and mixing effect in the screw channel. It is necessary to consider the non-Newtonian properties of polymer melts when designing extrusion screw. The TRT−LBM simulation results of the flow pattern agree well with the visualization experimental results of Yao et al. This study can provide a reference for the application of LBM in the chemical industry.

AUTHOR INFORMATION

Corresponding Author

Zhuo Meng − *College of Mechanical Engineering, Donghua University, Shanghai 201620, China*; Email: mz@dhu.edu.cn

Authors

Liguo Liu − *College of Mechanical Engineering, Donghua University, Shanghai 201620, China*; orcid.org/0000-0002-5370-3397

Yujing Zhang − *College of Mechanical Engineering, Donghua University, Shanghai 201620, China*

Yize Sun − *College of Mechanical Engineering, Donghua University, Shanghai 201620, China*

Complete contact information is available at: https://pubs.acs.org/10.1021/acsomega.3c06663

Notes

The authors declare no competing financial interest.

ACKNOWLEDGMENTS

This work was supported by the International Cooperation Fund of Science and Technology Commission of Shanghai municipality (21130750100).

REFERENCES

(1) Tadmor, Z.; Klein, I. *Engineering principles of plasticating extrusion*; Van Nostrand Reinhold Company: New York, 1970.

(2) Marschik, C.; Roland, W.; Miethlinger, J. A Network-Theory-Based Comparative Study of Melt-Conveying Models in Single-Screw Extrusion: A. Isothermal Flow. *Polymers* **2018**, *10* (8), 929.

(3) McKelvey, J. M. Polymer Processing. Wiley: New York, USA, 1962.

(4) Yao, W. G.; Takahashi, K.; Koyama, K.; Dai, G. C. Design of a new type of pin mixing section for a screw extruder based on analysis of flow and distributive mixing performance. *Chem. Eng. Sci.* **1997**, *52* (1), 13−21.

(5) Yao, W. G.; Takahashi, K.; Abe, Y. Analytical Study on Flow and Distributive Mixing of a New Type Pin Mixing Section for Screw Extruder. *Int. Polym. Process.* **1996**, *11* (3), 222−227.

(6) Horiguchi, H.; Takahashi, K.; Yokota, T. Numerical Simulation of the Flow Field in the Mixing Section of a Screw Extruder by the Lattice Gas Automata Method. *J. Chem. Eng. Jpn.* **2003**, *36* (1), 110−113.

(7) Buick, J. M.; Cosgrove, J. A. Numerical simulation of the flow field in the mixing section of a screw extruder by the lattice Boltzmann model. *Chem. Eng. Sci.* **2006**, *61* (10), 3323−3326.

(8) Buick, J. M.; Boyd, J. Non-Newtonian shear thinning flow in a single-screw extruder. *WSEAS Trans. Fluid Mech.* **2006**, *1* (8), 844−859.

(9) Buick, J. M. Lattice Boltzmann simulation of power-law fluid flow in the mixing section of a single-screw extruder. *Chem. Eng. Sci.* **2009**, *64* (1), 52−58.

(10) Qian, Y. H.; D'Humières, D.; Lallemand, P. Lattice bgk models for navier-stokes equation. *Europhys. Lett.* **1992**, *17* (6), 479−484.

https://doi.org/10.1021/acsomega.3c06663
ACS Omega 2023, 8, 47991−48018

(11) Guo, Z.; Chang, S. *Lattice Boltzmann Method and Its Applications in Engineering*; World Scientific, 2013.
(12) Lallemand, P.; Luo, L. S. Theory of the lattice boltzmann method: dispersion, dissipation, isotropy, galilean invariance, and stability. *Phys. Rev. E: Stat. Phys., Plasmas, Fluids, Relat. Interdiscip. Top.* **2000**, *61* (6), 6546−6562.
(13) An, B.; Bergada, J. M.; Mellibovsky, F.; Sang, W. M. New applications of numerical simulation based on lattice boltzmann method at high reynolds numbers. *Comput. Math. Appl.* **2020**, *79* (6), 1718−1741.
(14) Fakhari, A.; Lee, T. Multiple-relaxation-time lattice boltzmann method for immiscible fluids at high reynolds numbers. *Phys. Rev. E: Stat., Nonlinear, Soft Matter Phys.* **2013**, *87* (2), 023304.
(15) Wu, Y.; Gui, N.; Yang, X.; Tu, J.; Jiang, S. A decoupled and stabilized lattice boltzmann method for multiphase flow with large density ratio at high reynolds and weber numbers. *J. Comput. Phys.* **2021**, *426*, 109933.
(16) Park, J. W.; Choi, H. G. Simulation of turbulent flow over staggered tube bundles using multi-relaxation time lattice boltzmann method. *ATW, Int. Z. Kernenerg.* **2014**, *59* (2), 96−105.
(17) Boyd, J.; Buick, J. M. Three-dimensional modelling of the human carotid artery using the lattice Boltzmann method: I. Model and velocity analysis. *Phys. Med. Biol.* **2008**, *53* (20), 5767−5779.
(18) Chang, S. C.; Chen, C. L.; Cheng, S. C. Analysis of convective heat transfer improved impeller stirred tanks by the lattice Boltzmann method. *Int. J. Heat Mass Tran.* **2015**, *87*, 568−575.
(19) Chen, C. L.; Chang, S. C.; Chen, C. Y. Lattice boltzmann simulation of convective heat transfer of non-newtonian fluids in impeller stirred tank. *Appl. Math. Model.* **2017**, *46*, 519−535.
(20) Ohta, M.; Nakamura, T.; Yoshida, Y.; Matsukuma, Y. Lattice Boltzmann simulations of viscoplastic fluid flows through complex flow channels. *J. Non-Newtonian Fluid Mech.* **2011**, *166* (7−8), 404−412.
(21) Tang, G. H.; Wang, S. B.; Ye, P. X.; Tao, W. Q. Bingham fluid simulation with the incompressible lattice Boltzmann model. *J. Non-Newtonian Fluid Mech.* **2011**, *166* (1−2), 145−151.
(22) Qi, Z.; Kuang, S.; Qiu, T.; Yu, A. Lattice boltzmann investigation on fluid flows through packed beds: interaction between fluid rheology and bed properties. *Powder Technol.* **2020**, *369*, 248−260.
(23) Qi, Z.; Kuang, S. B.; Yu, A. B. Lattice boltzmann investigation of non-newtonian fluid flow through a packed bed of uniform spheres. *Powder Technol.* **2019**, *343*, 225−236.
(24) Qi, Z.; Kuang, S. B.; Rong, L. W.; Yu, A. B. Lattice boltzmann investigation of the wake effect on the interaction between particle and power-law fluid flow. *Powder Technol.* **2018**, *326*, 208−221.
(25) Deng, L.; Liang, J.; Zhang, Y.; Zhou, H.; Huang, Z. Efficient numerical simulation of injection mold filling with the lattice Boltzmann method. *Eng. Comput.* **2017**, *34* (2), 307−329.
(26) Mohebbi, R.; Nazari, M.; Kayhani, M. H. Comparative study of forced convection of a power-law fluid in a channel with a built-in square cylinder. *J. Appl. Mech. Tech. Phys.* **2016**, *57* (1), 55−68.
(27) Behrend, O.; Harris, R.; Warren, P. B. Hydrodynamic behavior of lattice Boltzmann and lattice Bhatnagar-Gross-Krook models. *Phys. Rev. E: Stat. Phys., Plasmas, Fluids, Relat. Interdiscip. Top.* **1994**, *50* (6), 4586−4595.
(28) Niu, X. D.; Shu, C.; Chew, Y. T.; Wang, T. G. Investigation of Stability and Hydrodynamics of Different Lattice Boltzmann Models. *J. Stat. Phys.* **2004**, *117* (3−4), 665−680.
(29) Gabbanelli, S.; Drazer, G.; Koplik, J. Lattice Boltzmann method for non-Newtonian (power-law) fluids. *Phys. Rev. E: Stat., Nonlinear, Soft Matter Phys.* **2005**, *72*, 046312.
(30) Yoshino, M.; Hotta, Y.; Hirozane, T.; Endo, M. A numerical method for incompressible non-Newtonian fluid flows based on the lattice Boltzmann method. *J. Non-Newtonian Fluid Mech.* **2007**, *147* (1−2), 69−78.
(31) Wang, L.; Mi, J.; Meng, X.; Guo, Z. A Localized Mass-Conserving Lattice Boltzmann Approach for Non-Newtonian Fluid Flows. *Commun. Comput. Phys.* **2015**, *17* (4), 908−924.
(32) Wang, C. H.; Ho, J. R. A lattice Boltzmann approach for the non-Newtonian effect in the blood flow. *Comput. Math. Appl.* **2011**, *62* (1), 75−86.
(33) Chai, Z.; Shi, B.; Guo, Z.; Rong, F. Multiple-relaxation-time lattice Boltzmann model for generalized Newtonian fluid flows. *J. Non-Newtonian Fluid Mech.* **2011**, *166* (5−6), 332−342.
(34) Li, Q.; Hong, N.; Shi, B.; Chai, Z. Simulation of Power-Law Fluid Flows in Two-Dimensional Square Cavity Using Multi-Relaxation-Time Lattice Boltzmann Method. *Commun. Comput. Phys.* **2014**, *15* (1), 265−284.
(35) Bisht, M.; Patil, D. V. Assessment of multiple relaxation time-lattice boltzmann method framework for non-newtonian fluid flow simulations. *Eur. J. Mech. B Fluid* **2021**, *85*, 322−334.
(36) Chen, S. G.; Sun, Q. C.; Jin, F.; Liu, J. G. Simulations of Bingham plastic flows with the multiple-relaxation-time lattice Boltzmann model. *Sci. China: Phys., Mech. Astron.* **2014**, *57* (3), 532−540.
(37) Grasinger, M.; Overacker, S.; Brigham, J. Numerical Investigation of the Accuracy, Stability, and Efficiency of Lattice Boltzmann Methods in Simulating Non-Newtonian Flow. *Comput. Fluid* **2018**, *166*, 253−274.
(38) Chen, S. G.; Zhang, C. H.; Feng, Y. T.; Sun, Q. C.; Jin, F. Three-dimensional simulations of Bingham plastic flows with the multiple-relaxation-time lattice Boltzmann model. *Eng. Appl. Comput. Fluid Mech.* **2016**, *10*, 346−358.
(39) Timm Krüger; Kusumaatmaja, H.; Kuzmin, A.; Shardt, O.; Viggen, E. M. *The Lattice Boltzmann Method-Principles and Practice*; Springer International Publishing Switzerland, 2016.
(40) Ginzburg, I.; Verhaeghe, F.; d'Humières, D. Two-Relaxation-Time Lattice Boltzmann Scheme: About Parametrization, Velocity, Pressure and Mixed Boundary Conditions. *Commun. Comput. Phys.* **2008**, *3* (2), 427−478.
(41) Ginzburg, I. Truncation errors, exact and heuristic stability analysis of two-relaxation-times lattice boltzmann schemes for anisotropic advection-diffusion equation. *Commun. Comput. Phys.* **2012**, *11* (5), 1439−1502.
(42) d'Humières, D.; Ginzburg, I. Viscosity independent numerical errors for lattice boltzmann models: from recurrence equations to "magic" collision numbers. *Comput. Math. Appl.* **2009**, *58* (5), 823−840.
(43) Luo, L. S.; Liao, W.; Chen, X.; Peng, Y.; Zhang, W. Numerics of the lattice boltzmann method: effects of collision models on the lattice boltzmann simulations. *Phys. Rev. E: Stat., Nonlinear, Soft Matter Phys.* **2011**, *83* (5), 056710.
(44) Mao, S.; Wang, X.; Sun, D.; Wang, J. Numerical modeling of dendrite growth in a steady magnetic field using the two relaxation times lattice boltzmann-phase field model. *Comput. Mater. Sci.* **2022**, *204*, 111149.
(45) Lee, Y. K. Comparative study of two-relaxation time lattice boltzmann and finite element methods for a planar 4:1 contraction flow: a newtonian fluid at finite reynolds numbers. *Korea Aust. Rheol. J.* **2023**, *35* (1), 47−54.
(46) Zhan, C.; Chai, Z.; Shi, B. A two-relaxation-time lattice Boltzmann study on the Soret and Dufour effects of double-diffusive convection over a rough surface. *Appl. Math. Model.* **2022**, *106*, 1−29.
(47) Cui, X.; Wang, Z.; Yao, X.; Liu, M.; Yu, F.; Beauwens, R. A coupled two-relaxation-time lattice boltzmann-volume penalization method for flows past obstacles. *Math. Comput. Simulat.* **2022**, *198*, 85−105.
(48) Quarteroni, A.; Tuveri, M.; Veneziani, A. Computational vascular fluid dynamics: problems, models and methods. *Comput. Visual Sci.* **2000**, *2* (4), 163−197.
(49) Bird, R. B.; Dai, G. C.; Yarusso, B. J. The Rheology and Flow of Viscoplastic Materials. *Rev. Chem. Eng.* **1983**, *1* (1), 1−70.
(50) Papanastasiou, T. C. Flows of Materials with Yield. *J. Rheol.* **1987**, *31* (5), 385−404.
(51) Bhatnagar, P. L.; Gross, E. P.; Krook, M. K. A Model for Collision Processes in Gases. I. Small Amplitude Processes in Charged

https://doi.org/10.1021/acsomega.3c06663
ACS Omega 2023, 8, 47991−48018

and Neutral One-Component Systems. *Phys. Rev.* **1954**, *94* (3), 511−525.
(52) Proefschrift, A.; Monim, A.; Ali, M.; Artoli, M. H. Mesoscopic computational haemodynamics. Ponsen en Looijen, 2003.
(53) Ziegler, D. P. Boundary conditions for Lattice Boltzmann simulations. *J. Stat. Phys.* **1993**, *71* (5−6), 1171−1177.
(54) He, X.; Zou, Q.; Luo, L. S.; Dembo, M. Analytic solutions of simple flows and analysis of nonslip boundary conditions for the lattice Boltzmann BGK model. *J. Stat. Phys.* **1997**, *87* (1−2), 115−136.
(55) Bell, B. C.; Surana, K. S. p-Version least squares finite element formulation for two-dimensional incompressible Nnewtonian and non-Newtonian non-isothermal fluid flow. *Comput. Struct.* **1995**, *54* (1), 83−96.
(56) Neofytou, P. A 3rd order upwind finite volume method for generalised Newtonian fluid flows. *Adv. Eng. Software* **2005**, *36* (10), 664−680.
(57) Ginzburg, I.; d'Humières, D.; Kuzmin, A. Optimal Stability of Advection-Diffusion Lattice Boltzmann Models with Two Relaxation Times for Positive/Negative Equilibrium. *J. Stat. Phys.* **2010**, *139* (6), 1090−1143.
(58) Suga, S. Stability and accuracy of Lattice Boltzmann Schemes for anisotropic advection-diffusion equations. *Int. J. Mod. Phys. C* **2009**, *20* (04), 633−650.

https://doi.org/10.1021/acsomega.3c06663
ACS Omega 2023, 8, 47991−48018